Journal of Marine Systems 189 (2019) 98–115

Contents lists available at ScienceDirect

Journal of Marine Systems

journal homepage: www.elsevier.com/locate/jmarsys

# The future regime of Atlantic nutrient supply to the Northwest European Shelf

M. Mathis[a,*], A. Elizalde[b], U. Mikolajewicz[a]

[a] Max-Planck-Institute for Meteorology, Bundesstr. 53, 20146 Hamburg, Germany
[b] Institute of Oceanography, University of Hamburg, Bundesstr. 53, 20146 Hamburg, Germany

ARTICLE INFO

*Keywords:*
Climate change
Northwest European Shelf
North Sea
Primary production
Dynamical downscaling
Ocean-atmosphere coupling

ABSTRACT

Downscaling simulations for emission scenario RCP8.5 with a regionally coupled ocean-atmosphere climate system model indicate a regime shift in the dynamics of Atlantic nutrient supply to the Northwest European Shelf. Reduced winter convection in the Northeast Atlantic leads to a substantial decrease in upper ocean nutrient concentrations. Yet, vertical mixing processes at the shelf break maintain a connection to nutrient-enriched subpycnocline water masses and decouple the nutrient supply to the shelf from upper ocean conditions in the North Atlantic. As a consequence, primary production on the shelf does not weaken as strongly as it was expected from declining nutrient concentrations in the open ocean. Furthermore, nutrient fluxes to the shelf become increasingly variable due to a positive feedback between the winter mixed layer depth near the shelf break and the density of the upper water column, making the productivity on the shelf more sensitive to the major modes of variability in the North Atlantic.

## 1. Introduction

Atlantic water masses flushing the Northwest European Shelf (NWES) were found to be the major source of oceanic nutrients to fuel marine primary production in open shelf areas (e.g. Brion et al., 2004; Vermaat et al., 2008; Thomas et al., 2010). Various phenomena such as wind-driven surface flow, instabilities of the slope current and breaking internal waves induce enhanced vertical mixing along the continental margin and continuous ocean-shelf exchange (e.g. White and Bowyer, 1997; Huthnance et al., 2009; Simpson and Sharples, 2012). Earth system models consistently project future decreases in ocean mixed layer depth (MLD) in the subpolar North Atlantic as a response to anthropogenic global warming (e.g. Bopp et al., 2001, 2013; Steinacher et al., 2010; Yool et al., 2015; Fu et al., 2016; Alexander et al., 2018). Reduced winter convection in the ocean limits the amount of nutrients mixed to the euphotic zone from nutrient-rich intermediate depths (e.g. Holliday, 2003; Williams et al., 2011). This physical mechanism is mainly governed by the projected warming and freshening of the upper ocean and its impact hence scales well among different forcing scenarios.

A central question is thus, how these changes in the North Atlantic would affect the nutrient supply to the NWES and thereby its biologically rich ecosystem. The conventional approach to address this question is a dynamical downscaling of global climate projections by regional circulation models which can afford higher grid resolutions than global models and have a more appropriate process representation to simulate shelf sea dynamics. Nevertheless, large uncertainties in downscaled future changes are related to the choices of the forcing global model, the particular realization and the downscaling regional model system. Aspects of such uncertainties are indicated, for instance, by wide spreads in projected North Sea primary production and $CO_2$ uptake (Holt et al., 2012, 2016; Wakelin et al., 2012; Gröger et al., 2013; Chust et al., 2014; Schrum et al., 2016; Mathis et al., 2018). Furthermore, downscaled changes in several key parameters affecting primary production, such as water temperature, seasonal stratification and ocean circulation, sensitively depend on coupled ocean-atmosphere interaction both in the NWES and subpolar North Atlantic (Schrum, 2017; Mathis et al., 2018). Most previous climate change impact studies, however, are based on uncoupled ocean simulations with limited domain sizes, leaving their results strongly influenced by the prescribed atmospheric and oceanic boundary conditions.

The present study builds on the findings by Mathis et al. (2018) and presents high-resolution coupled ocean-atmosphere downscalings for the NWES, driven by global climate projections according to emission scenarios RCP4.5 and RCP8.5 (Representative Concentration Pathways, Intergovernmental Panel on Climate Change Assessment Report 5). The peculiarity of the applied model system is that its ocean component is

* Corresponding author.
*E-mail addresses:* moritz.mathis@mpimet.mpg.de (M. Mathis), alberto.elizalde@uni-hamburg.de (A. Elizalde), uwe.mikolajewicz@mpimet.mpg.de (U. Mikolajewicz).

https://doi.org/10.1016/j.jmarsys.2018.10.002
Received 26 January 2018; Received in revised form 1 October 2018; Accepted 11 October 2018
Available online 19 October 2018
0924-7963/ © 2018 Elsevier B.V. All rights reserved.

global but runs on a stretched grid configuration, achieving higher resolutions in the North Atlantic and NWES regions without the need for prescribed open boundary conditions. The unbounded ocean domain allows for a consistent simulation of climatic signals propagating from the open Atlantic to the shelf and thus is particularly advantageous for investigating NWES climate change impacts driven by changes in the North Atlantic circulation. Pätsch et al. (2017) demonstrated the model skills for capturing oceanographic features most relevant for ecosystem modeling in the transition zone from deep-ocean to shallow-shelf conditions, such as water mass distribution and thermal stratification.

In the present study an ensemble of three realizations by the parent global climate model per scenario has been downscaled for the 21st century to address uncertainties due to internal variability. Most previous climate change impact studies and assessment reports for the European seas are restricted to the 21st century (e.g. Ådlandsvik, 2008; Gröger et al., 2013; Wakelin et al., 2015; Holt et al., 2016; Schrum et al., 2016; Mathis et al., 2018), as is the majority of available global model output that drives downscaling simulations. The variety of involved downscaling approaches, forcing global models and future scenarios help identify uncertainties in the simulated changes as well as challenges and limitations for early warning systems. To put our ensemble simulations into context, the downscaling model system is described and evaluated in Section 2. Change signals for the 21st century are presented in Section 3, including an estimation of various sources of uncertainty. A key point of our analysis is the change in NWES primary production and the underlying physical driving mechanisms, including exchange processes between the shelf and the open Atlantic. More detailed results are presented for the northern North Sea, as this is the largest connected shelf area predominantly influenced by Atlantic inflow. Our simulations indicate that towards the end of the 21st century the shoaling of the North Atlantic mixed layer in scenario RCP8.5 provokes a regime shift in the dynamics of the Atlantic nutrient supply to the shelf. In Section 4 we extend one realization for each scenario beyond the year 2100 and explore why after the regime shift the nutrient availability on the shelf does not decline as strongly as in the Northeast (NE) Atlantic and why nutrient fluxes onto the shelf are characterized by enhanced interannual and multidecadal variability. Main results and conclusions are summarized in Section 5.

## 2. Methods

### 2.1. Model description

The applied downscaling tool is a regionally coupled ocean-atmosphere climate system model (Mikolajewicz et al., 2005; Elizalde Arellano, 2011; Sein et al., 2015), consisting of the global ocean-sea ice model MPIOM, the global biogeochemistry model HAMOCC, the regional atmosphere model REMO and the hydrological discharge model HD. This model system is the same as used in Mathis et al. (2018) but has been launched here with higher spatial and temporal resolutions. A brief description of the individual model components is given in the following subsection.

#### 2.1.1. Components

MPIOM (Maier-Reimer, 1997; Marsland et al., 2003; Jungclaus et al., 2013) is the ocean-sea ice component of the global earth system model MPI-ESM of the Max-Planck-Institute for Meteorology in Hamburg. The primitive equations of oceanic motion are discretized on an Arakawa C-grid with z-coordinates and free surface. Hydrostatic and Boussinesq approximations are applied. A second order total variation diminishing scheme (Sweby, 1984) is used to simulate tracer and momentum advection. Vertical mixing is implemented after Pacanowski and Philander (1981). The full luni-solar tidal potential is calculated according to Thomas et al. (2001).

In the present study MPIOM has been run on a stretched grid configuration with non-diametrical poles located over Central Europe and North America (Fig. 1). We use a nominal horizontal grid resolution of 0.6°, yielding mesh sizes of about 5 to 12 km on the NWES and less than 20 km in the subpolar North Atlantic. The vertical is resolved by 30 levels with 8 levels in the upper 100 m.

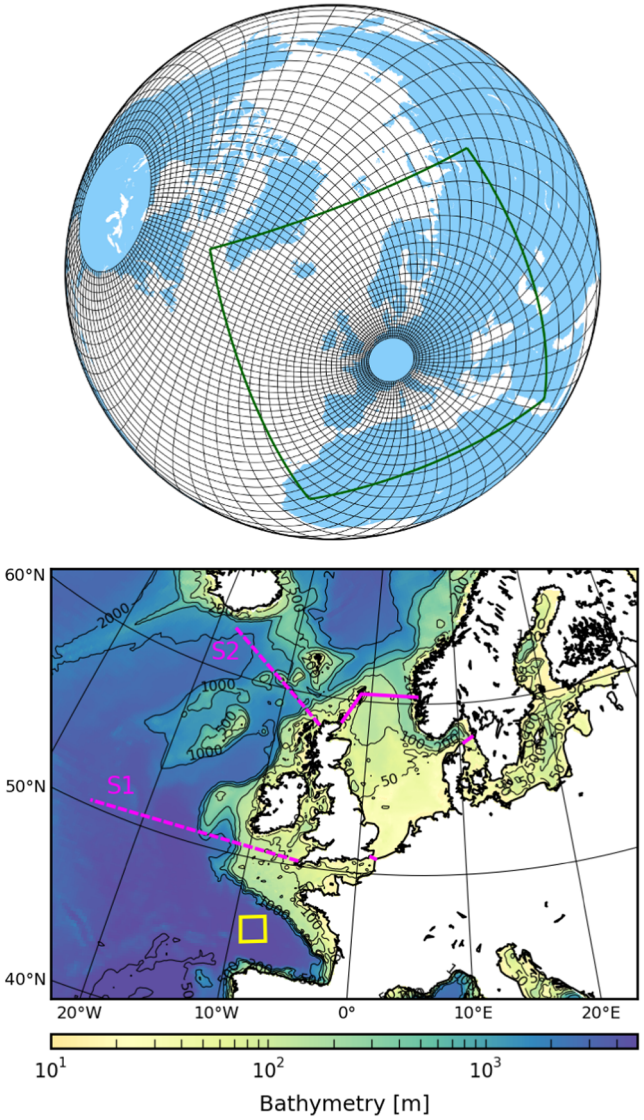


**Fig. 1.** Top: Grid configuration of the global ocean model MPIOM (black lines, every 7th grid line is shown), providing a higher horizontal grid resolution in the North Atlantic and NWES. Green lines represent the boundaries of the regional atmosphere model REMO. Bottom: Bathymetry of the Northwest European Shelf. Isobaths [m]: 50, 100, 200, 500, 1000, 2000, 5000. Magenta solid lines: Region used for spatial averages over the North Sea. The northern boundary is used to calculate fluxes via the Fair-Isle Current, the East-Shetland Flow and the inflow along the western side of the Norwegian Trench. The northern and southern North Sea areas are separated by the 50 m isobath. Magenta dashed lines: Transects crossing the shelf break at 50.5°N (S1) and 59°N (S2). Yellow box: Region used for time series near the Bay of Biscay shown in Fig. 18.

Biogeochemical processes in the ocean are simulated by the Hamburg Ocean Carbon Cycle model HAMOCC (Maier-Reimer et al., 2005; Ilyina et al., 2013). Marine biology dynamics is represented by nutrients, phytoplankton, zooplankton, detritus, and dissolved organic matter (Six and Maier-Reimer, 1996). Biogeochemical cycles and trophic levels are connected by nutrient uptake and remineralization of organic matter (Six and Maier-Reimer, 1996; Kloster et al., 2006). A sediment module accounts for deposition and dissolution processes as well as the biogeochemistry of pore water in the upper bioturbated sediments (Heinze et al., 1999). Sediment resuspension in the model configuration described here is based on the concept of incipient

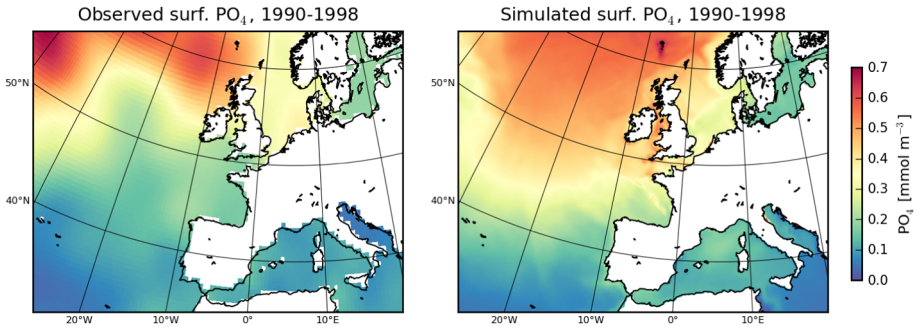


**Fig. 2.** Annual surface $PO_4$ concentrations over the period 1990–1998. Left: Observational data according to WOCE Global Hydrographic Climatology (Gouretski and Koltermann, 2004). Right: Simulation ensemble mean of three realizations.

motion (Wilcock, 2004). A brief description is given in Appendix A. Tracer transport is simulated by MPIOM.

The regional atmosphere model REMO (Jacob and Podzun, 1997; Jacob et al., 2001) has been run with a uniform resolution of about 25 km and 27 hybrid levels covering the EURO-CORDEX domain (e.g. Kotlarski et al., 2014), see also Fig. 1. MPIOM is interactively coupled with REMO over the domain of the atmosphere model at a coupling time step of 1 h. Sea surface fluxes of heat, momentum, and freshwater are transferred to MPIOM by the OASIS3 coupler (Valcke, 2013). In turn, sea surface temperature (SST) and sea ice cover are passed from MPIOM to REMO. At the land-atmosphere interface a simple bucket scheme is applied for the treatment of soil hydrology. Freshwater drainage and runoff are calculated by the hydrological discharge model HD (Hagemann and Dümenil-Gates, 2001).

6-hourly atmospheric forcing is derived from the atmosphere component of the driving global climate model. Here we use a set of CMIP5 (Coupled Model Intercomparison Project Phase 5 of the World Climate Research Programme) simulations by the global earth system model MPI-ESM (Max-Planck-Institute Earth System Model) in its low resolution version (LR; Giorgetta et al., 2013). The forcing is used as lateral boundary conditions for REMO and as input for the calculation of atmosphere-ocean fluxes from standard bulk formulas by MPIOM outside the domain covered by REMO.

### 2.2. Experiment design

Our simulations cover the historical period 1920–2005 and the scenario period 2006–2100 with prescribed atmospheric greenhouse gas concentrations according to emission scenarios RCP4.5 and RCP8.5. For the historical period as well as for each scenario we downscaled an ensemble of three MPI-ESM realizations. The MPI-ESM realizations branch from different years of the corresponding preindustrial control run and hence differ only in their initial conditions used for the initial year 1850. The downscaling of the first MPI-ESM realization from 1850 to 1919 provided initial conditions for all three downscaling ensemble members starting in 1920. The first 41 years are considered as spin-up for the ensemble member. The total spin-up of 111 years helped to minimize the effect of model drift. To allow to account for remaining model drift especially in the deep ocean properly, the preindustrial control run has also been downscaled. For physical conditions there is no discernable drift in the upper North Atlantic, e.g. for sea surface temperature, salinity and elevation or the strengths of the subpolar gyre (SPG) and Meridional Overturning Circulation (MOC), indicating reasonable ocean-atmosphere equilibrium. Sub-mixed layer nutrient concentrations, however, show a negative drift of about 0.05 mmol P $m^{-3}$ 100$yr^{-1}$ and 0.8 mmol N $m^{-3}$ 100$yr^{-1}$ for dissolved phosphate and nitrate, respectively. Therefore, in the results sections (Sections 3 and 4), time series of the control run are shown together with the scenario runs.

Historical riverine nutrient concentrations are provided for the North Sea (Pätsch and Lenhart, 2004), Baltic Sea (Savchuk et al., 2012), and Mediterranean Sea (Ludwig et al., 2009), while future concentrations follow a white noise distribution with mean and variance of the period 2001–2010 from the cited observations. Atmospheric dust deposition follows a present-day eolian climatology (Mahowald et al., 2006).

### 2.3. Evaluation

Previous studies employing MPIOM/HAMMOC in similar configurations driven by prescribed atmospheric forcing have already evaluated physical and biogeochemical conditions on the NWES (Gröger et al., 2013; Mathis et al., 2015; Pätsch et al., 2017; Hátún et al., 2017). Therefore, we restrict the evaluation in the present study to phosphate ($PO_4$) concentrations, primary production and sediment deposition of organic material.

The model has a nearly constant N:P ratio in the region of interest. In our analysis we therefore use $PO_4$ as a representative of nutrients in general. For the northern North Sea, which is analyzed in more detail, this is a reasonable approximation because of the predominance of Atlantic water masses with winter N:P ratio close to 16 (e.g. Radach and Lenhart, 1995; Radach and Pätsch, 1997; Brion et al., 2004). Simulated pre-bloom $PO_4$ concentrations in the northern North Sea show a positive bias of about 0.1 mmol P $m^{-3}$ (Fig. 2) and in the NE Atlantic the transition zone from subtropical to subpolar water masses is displaced southward (Figs. 2 and 3), probably due to underestimated northward transport.

Simulated annual primary production in the northern North Sea amounts to 10.9 mol C $m^{-2}$ $yr^{-1}$ for 1971–2000, lying well within the observational range of 9–12 mol C $m^{-2}$ $yr^{-1}$ estimated from Van Beusekom and Diel-Christiansen (1994), Varela et al. (1995) and Capuzzo et al. (2018). Furthermore, the annual cycle given in Radach and Pätsch (1997), Moll (1998) and Luff and Moll (2004) agrees well in the timing and ratio of spring bloom and summer growth shown in Fig. 7.

For the period 1971–2000, simulated deposition rates of organic material in the North Sea amount to 0.10 –0.15 mol C $m^{-2}$ $yr^{-1}$. These values compare well with observation-based estimates of 0.13 mol C $m^{-2}$ $yr^{-1}$ (De Haas et al., 2002; Thomas et al., 2005).

### 2.4. Analysis

The study area of the NWES is shown in Fig. 1, indicating the regions used for spatial averages over the North Sea and a subregion in the Bay of Biscay (see Section 4). The northern and southern North Sea areas are separated by the 50 m isobath.

Climate change signals of the scenario simulations are calculated by comparing climatologies for the end of the 21st century (2071–2100) with the end of the last century (1971–2000). Statistical significance is derived from the variance of the preindustrial control run. Uncertainties due to internal variability of the parent global model are estimated by the ensemble spread of the three realizations. This is a more meaningful

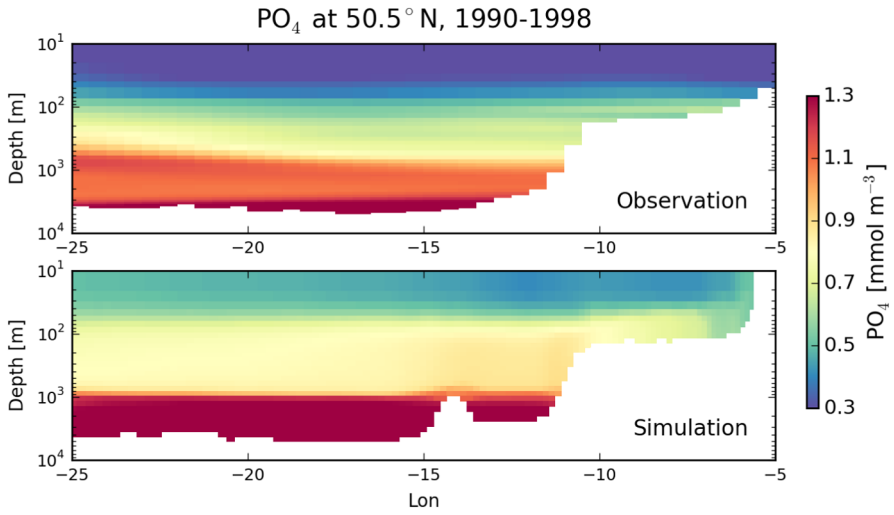


**Fig. 3.** Vertical distribution of annual $PO_4$ concentrations over the period 1990–1998 exemplified at 50.5°N (Fig. 1, S1). Top: Observational data according to WOCE Global Hydrographic Climatology (Gouretski and Koltermann, 2004). Bottom: Simulation ensemble mean of three realizations. Note the logarithmic depth scale.

measure for a small ensemble than the standard deviation. When addressing uncertainties due to internal variability we therefore always refer to the maximum ensemble spread.

## 3. Projected changes during the 21st century

### 3.1. Changes in physical conditions

In our simulations, SST on the NWES rises during the 21st century between 0.9 –1.1 K for RCP4.5 and 1.6 –2.3 K for RCP8.5 (Fig. 4a) with about 0.4 K ensemble spread. In the northern North Sea, SST increases by 1.0 and 2.0 K for the two scenarios, with similar ensemble spread. In the seasonally stratified areas the warming surface water induces a strengthening in the maximum vertical density gradient due to the nonlinear dependence of the water density on temperature. The intensity of the summer (JJA) pycnocline in the northern North Sea increases by about 8 g $m^{-4}$ for scenario RCP4.5 and 16 g $m^{-4}$ for RCP8.5 (6 g $m^{-4}$ ensemble spread), while its depth decreases by about 0.8 m and 1.6 m (1.2 m ensemble spread).

In open shelf regions, sea surface salinity (SSS) decreases by about 0.3 for RCP4.5 and 0.5 for RCP8.5 (Fig. 4b) with 0.1 ensemble spread. This is mainly a consequence of the freshening of the inflow from the Atlantic. Increased river runoff by about 6% and 12% for the two scenarios (8% ensemble spread) causes an enhanced freshening along the continental coast, the Norwegian Coastal Current and in the Baltic Sea.

The inflow of Atlantic water masses to the northern North Sea

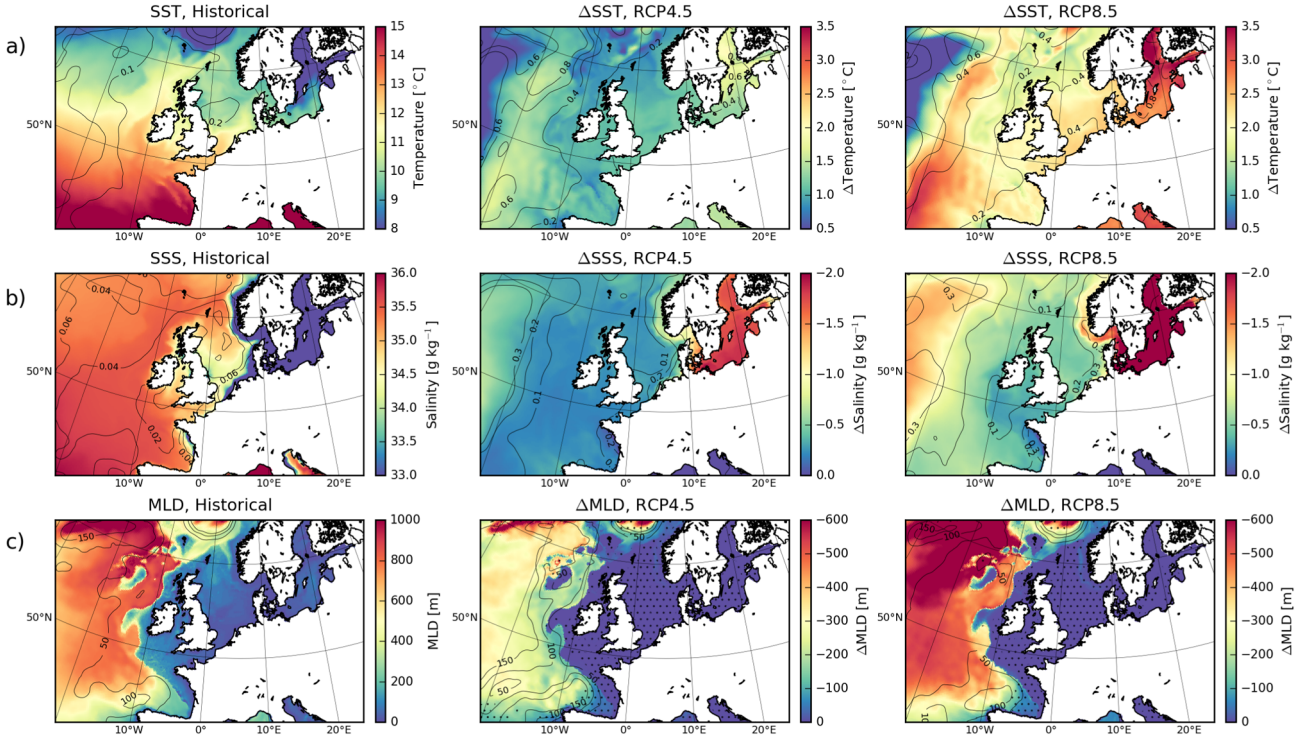


**Fig. 4.** Historical mean (1971–2000; left column) as well as 100-year change signals (2071–2100 minus 1971–2000) according to scenarios RCP4.5 (middle column) and RCP8.5 (right column) for a) annual SST, b) annual SSS and c) maximum winter MLD (March). Colors: Ensemble mean over three realizations. Contours: Ensemble spread between minimum and maximum realizations. Dotted areas mark changes less than 95% significance.

weakens. For RCP8.5, net Atlantic winter inflow of about 1.5 Sv via the Fair-Isle Current, the East-Shetland Flow and the inflow along the western side of the Norwegian Trench decreases by 0.1 Sv (0.17 Sv ensemble spread), reflecting a general weakening of the northern North Sea circulation. This is consistent with results from previous studies (Mathis and Pohlmann, 2014; Tinker et al., 2016; Mathis et al., 2018). The changes in RCP4.5 go into the same direction, but are not statistically significant.

Off the continental shelf break the warming and freshening of the upper ocean induces a shoaling in maximum winter MLD (March) by up to 200 and 450 m for the two scenarios (Fig. 4c). MLD has been defined here as the depth where the potential water density has increased by 0.125 kg $m^{-3}$ from near-surface conditions (e.g. Monterey and Levitus, 1997; Suga et al., 2004; Williams et al., 2006). The considerable ensemble variability west of 20°W arises from high internal variability in the simulated strength and extension of the SPG, which induces substantial variations in the physical and biogeochemical conditions of NE Atlantic water masses (Hátún et al., 2005; Johnson et al., 2013; Häkkinen et al., 2013). Similarly large ensemble variability is therefore also evident for changes in Atlantic nutrient concentrations (Fig. 5a), which are presented in the next subsection.

### 3.2. Changes in nutrient transports and primary production

Nutrients are advected to the subpolar North Atlantic via a subsurface nutrient stream associated with the western boundary current (e.g. Williams and Follows, 2003; Williams et al., 2006). Incorporation into the deep winter mixed layer transports the nutrients from intermediate depths to the biologically productive euphotic zone (e.g. Williams et al., 2000; Holliday, 2003; Williams et al., 2011). In the NE Atlantic, interannual correlations between simulated maximum winter (March) MLD and surface nutrient concentrations range between 0.7 and 0.95 for both present-day and future scenario conditions. The projected weakening of the SPG and MOC (by about 15 Sv and 8 Sv for RCP8.5, respectively) and in particular the shoaling of the MLD (Fig. 4c) thus substantially weaken the upward nutrient transports. For both scenarios, March surface $PO_4$ concentrations in the NE Atlantic decline by about 0.3 and 0.4 mmol P $m^{-3}$ (Fig. 5a).

The nutrient import from the NE Atlantic to the northern North Sea is reduced by about 14% for scenario RCP4.5 and 23% for RCP8.5 (28% ensemble spread). The strongest contribution to this reduction is from the declining nutrient concentrations of the inflowing Atlantic water masses (Fig. 6a). The considerable ensemble spread results from the high variability of associated volume fluxes with a standard deviation of about 30% of the mean (see also Hjøllo et al., 2009; Mathis et al., 2015; Marsh et al., 2017).

The reduced nutrient import lowers March nutrient concentrations in the northern North Sea by about 0.14 and 0.18 mmol P $m^{-3}$ (Fig. 5a) and causes continuous decreases in annual net primary production (Figs. 5b and 6b) and $CO_2$ uptake Appendix B. By the end of the century, the productivity is weakened by about 1.8 mol C $m^{-2}$ $yr^{-1}$ (17%) for RCP4.5 and 2.3 mol C $m^{-2}$ $yr^{-1}$ (21%) for RCP8.5 (0.7 mol C $m^{-2}$ $yr^{-1}$ ensemble spread).

Another major factor limiting productivity in the northern North Sea is the projected strengthening in the local seasonal stratification (Section 3.1), which affects the availability of remineralized nutrients above the thermocline. A minor limiting influence results from a slight increase in cloudiness by about 3% and 8% (5% ensemble spread), which reduces downward short wave radiation at the sea surface.

Considering the annual cycle of northern North Sea primary production (Fig. 7), maximum productivity during spring bloom is limited in the model by nutrient depletion in the euphotic zone and zooplankton grazing. The onset of the spring bloom does not change in the scenario runs since it is mainly governed by seasonally rising solar irradiance. Reduced wintertime nutrient concentrations, however, lead to a less intense and shorter (by 8–10 days) spring bloom (Fig. 7). During the following summer growth, phytoplankton growth and zooplankton grazing roughly balance due to continuous nutrient supply via remineralization of particulate organic matter and cross-pycnocline exchange. The enhanced stratification in the scenario runs (Section 3.1) reduces the cross-pycnocline upward nutrient transport, further weakening annual primary production. Simulated changes in the limitation factors for light and temperature (not shown) suggest that the positive effect of the projected SST increase (Section 3.1) and the negative effect of cloudiness (see above) approximately cancel over the total growing season.

### 3.3. Discussion

The projected warming of the upper ocean facilitates better growing conditions for plankton species and therefore affects the general decrease in primary production in a mitigating manner. Nevertheless, future changes in North Sea SST projected by previous climate change impact studies according to the A1B (IPCC AR4) scenario (e.g. Ådlandsvik, 2008; Holt et al., 2010; Gröger et al., 2013; Bülow et al., 2014; Mathis and Pohlmann, 2014) show a considerable spread, covered only by the full range of our RCP4.5 and RCP8.5 ensembles. The storyline of A1B emissions during the 21st century is approximately centered between RCP4.5 and RCP8.5 but the cited studies utilize different downscaling model systems, different forcing global models and

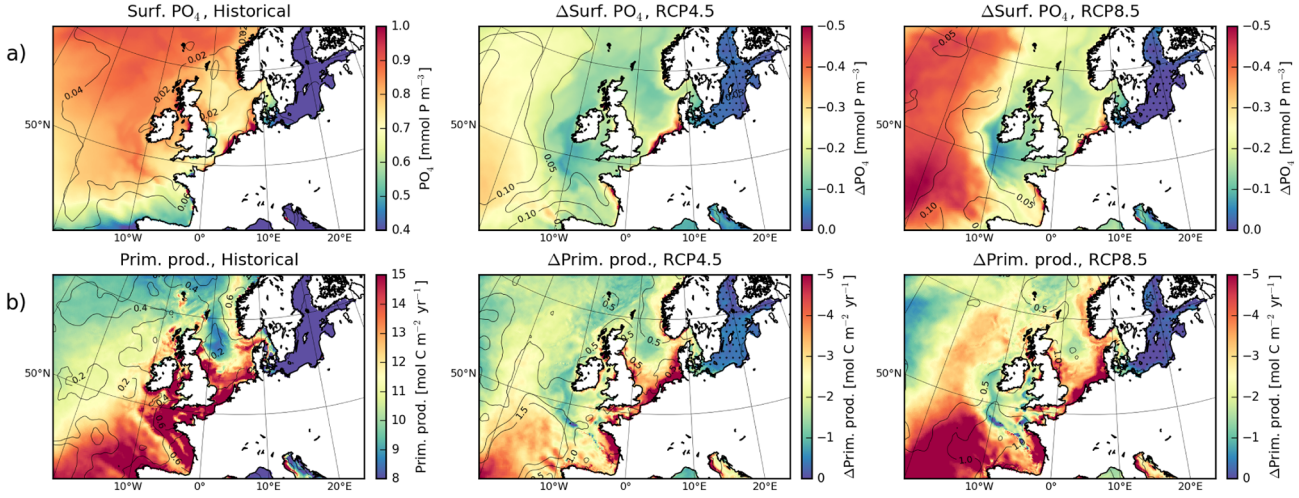


**Fig. 5.** As Fig. 4 but for a) pre-bloom surface $PO_4$ concentration (March) and b) depth-integrated annual net primary production.

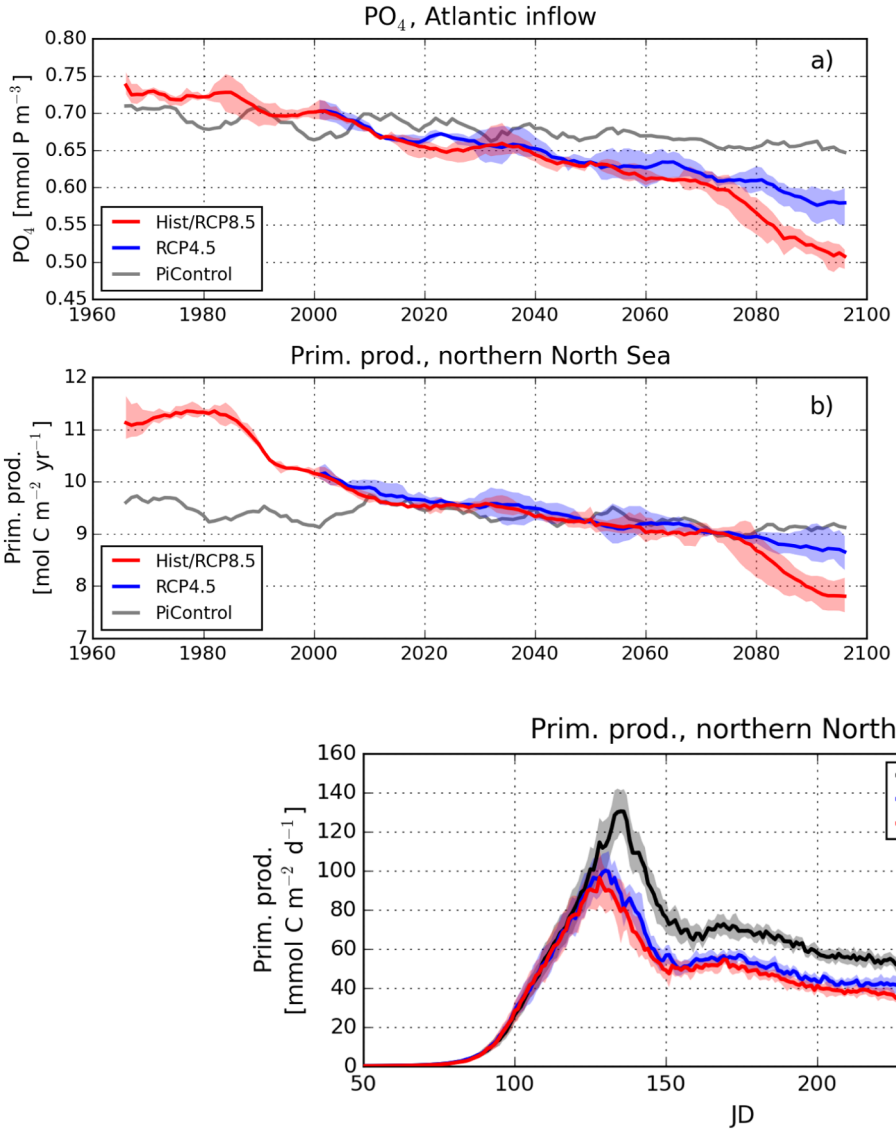


**Fig. 6.** Time series (10-year running means) of winter $PO_4$ concentrations of Atlantic inflow to the northern North Sea via the Fair-Isle Current, the East-Shetland Flow and the inflow along the western side of the Norwegian Trench (a) and northern North Sea depth-integrated net primary production (b). Gray line: pre-industrial control; blue line: ensemble mean RCP4.5; red line: ensemble mean historical and RCP8.5; shaded areas: ensemble spread between minimum and maximum values.




**Fig. 7.** Annual cycle of depth-integrated net primary production in the northern North Sea. Black line: ensemble mean historical 1971–2000. Blue line: ensemble mean RCP4.5 2071–2100. Red line: ensemble mean RCP8.5 2071–2100. Shaded areas: ensemble spread between minimum and maximum values.

different downscaling strategies, adding further uncertainties. RCP4.5 and RCP8.5 downscalings of one realization by Tian et al. (2016) are comparable to our ensemble members that show maximum warming, respectively, underlining the importance of taking internal model variability into account. Another realization by their model may have yielded lower trends. From a perturbed physics ensemble of the forcing global model, Tinker et al. (2016) obtained even stronger trends and uncertainties for A1B than our RCP8.5 ensemble suggests. Since they ran uncoupled downscalings, however, their results are strongly influenced by the prescribed atmospheric forcing (Mathis et al., 2018). The projected temperature increase in our simulations induces a strengthening of the seasonal stratification, consistent with results by Holt et al. (2010), Tian et al. (2016), Tinker et al. (2016) and Mathis et al. (2018).

Furthermore, our simulations indicate a weakening of biological productivity in the northern North Sea during the 21st century but basically no changes in the onset of the spring bloom or total duration of the annual production period. Considerable ranges in projected North Sea primary production were reported in several downscaling studies and reviews thereof (e.g. Wakelin et al., 2012; Gröger et al., 2013; Holt et al., 2016; Schrum et al., 2016; Mathis et al., 2018; Schrum, 2017), mainly rooted in the simulated or prescribed drop of Atlantic nutrient import. From the variety of used downscaling approaches and from the ensemble simulations presented here we are able to estimate different sources of uncertainty in the projected productivity changes. Taken into account the ensemble spreads shown in Figs. 6b and 7, uncertainties due to internal model variability are approximately 5–10% (range between minimum and maximum fractional changes) with respect to the forcing global model and 5% with respect to the downscaling (coupled) regional model, derived from a three-member ensemble downscaling of a single global realization presented in Mathis et al. (2018). Uncertainties due to the downscaling strategy addressed in Mathis et al. (2018) can be estimated to another 15% and uncertainties due to the chosen forcing global model and downscaling regional model amount to about 10–15% each (Wakelin et al., 2012; Holt et al., 2016). In the southern North Sea, additional uncertainties arise due to assumptions about future riverine nutrient loads.

In our RCP4.5 simulations the reductions in both northern North Sea productivity and Atlantic inflow nutrient concentrations are almost linear through the 21st century (Fig. 6), whereas the RCP8.5 simulations show a conspicuous increase in the rate of change during the last decades with an indication for enhanced variability. These disparities indicate that for scenario RCP8.5 the physical processes governing the nutrient budget on the shelf are subject to a regime shift. Because of its transitional character, however, the period 2071–2100 used in this

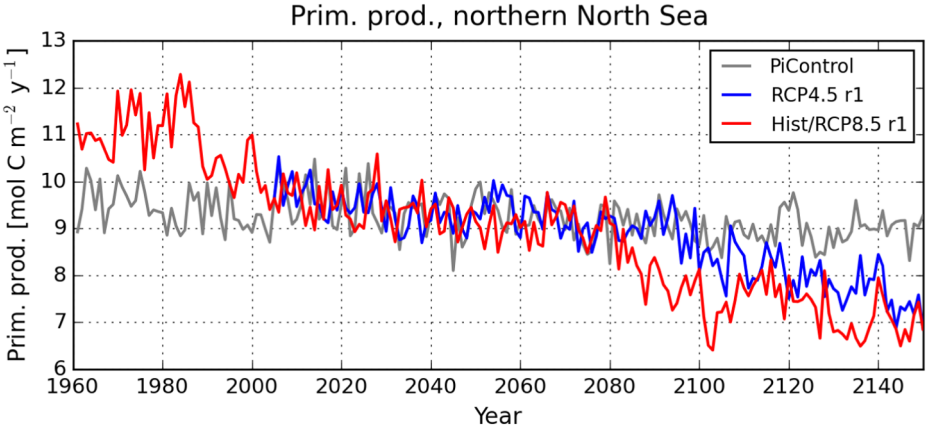


**Fig. 8.** Time series of annual depth-integrated net primary production in the northern North Sea. Gray: Preindustrial control. Blue: Scenario RCP4.5 (r1). Red: Historical period (r1) and scenario RCP8.5 (r1).

section is not optimally suited to investigate these processes. In the next section we therefore extend our simulations further into the future and explore the characteristics and driving mechanisms of the new regime.

## 4. Future regimes of Atlantic nutrient supply beyond 2100

During the last decades of the 21st century the decrease in northern North Sea primary production is accelerating in all realizations of scenario RCP8.5 (Fig. 6b). To further investigate this signal, we extended the first realizations (r1) of both scenarios as well as the control run by another 50 years into the future. From these extended simulations (Fig. 8) it becomes apparent that the strong productivity decrease in scenario RCP8.5 marks a transition into a new state of enhanced interannual to multidecadal variability (by 30%). In this section we investigate the underlying mechanisms by comparing the two 50-year periods 2011–2060 (near future), characterized by a steadily weakening productivity devoid of influences from high historical riverine nutrient loads, and 2101–2150 (far future).

### 4.1. Ocean-shelf nutrient front

During the near-future period, the distribution of surface nutrients at the end of winter shows higher concentrations in the open North Atlantic than on the NWES (Fig. 9a), similar to recent-past (Fig. 5a) and present-day conditions. Deep wintertime convection in the NE Atlantic (as deep as 800 m) brings nutrient-enriched water masses from intermediate depths to the upper ocean. Enhanced mixing at the shelf break (e.g. Huthnance, 1986; White and Bowyer, 1997; Huthnance et al., 2001) leads to locally enhanced nutrient concentrations at the surface.

In the far future, by contrast, wintertime convection in the NE Atlantic is strongly reduced (Fig. 9b), causing a drop in surface nutrient concentrations by about 0.4 mmol P m$^{-3}$ (Fig. 9a). In fact maximum MLD (March) does not reach deeper than the shelf edge at about 150–200 m (Fig. 9b), which is a region of several intense mixing processes. The abrupt change in bathymetry comes along with a change in the characteristic length scale and gives rise to exceptional forms of motion such as unstable along-shelf currents, interleaving water masses, and strong nonlinear internal tides and shelf waves (Huthnance, 1981). Upward mixing of subpycnocline waters maintains high nutrient concentrations at the shelf break (Fig. 10) and leads to the development of a nutrient front between the shelf break and the open Atlantic. From the shelf break the high nutrient concentrations spread onto the NWES, reverting the ocean-shelf gradient of nutrient concentrations (Fig. 9a). On-shelf transports via the wind-driven surface flow and the return flow which balances down-slope Ekman drain induced by the slope current have been identified as the most important mechanisms contributing to cross-shelf break transfer (Holt et al., 2009; Huthnance et al., 2009; Simpson and Sharples, 2012).

### 4.2. Enhanced interannual variability

In the far future the variability of end-of-winter surface nutrient concentrations is remarkably enhanced all along the continental margin (Fig. 11). The signal is strongest at the Celtic Shelf break but the region of increased variability also includes the northern North Sea, which is ventilated by Atlantic inflow. The southern North Sea is less influenced, as the effect of riverine nutrient input is dominant here.

The spatial correlation pattern of March surface $PO_4$ concentrations with the concentration at the Celtic Shelf break shows high positive correlations in the NE Atlantic and entire NWES (Fig. 12). Such a coherent pattern can only be produced by large-scale forcing mechanisms. To investigate the involved processes we therefore consider a transect at 50.5°N (S1 in Fig. 1), cutting through the region of maximum variability.

Time series of March surface $PO_4$ concentrations illustrate the full intensity of the variations at the Celtic Shelf break beyond the year 2100 (Fig. 13b, red line). Exceptionally low concentrations are associated with shallow winter mixed layers (Fig. 13a). In the adjacent Atlantic (blue line) nutrient concentrations keep falling, while on the shelf (green line) the nutrient decline is much weaker, setting up the ocean-shelf nutrient front (Section 4.1).

To investigate the mechanism responsible for the enhanced variability, we consider the vertical structure of the water column and perform a composite analysis of pronounced anomalies. The years used for the composites are selected from the $PO_4$ time series at the Celtic Shelf break shown in Fig. 13b (red curve). Years with anomalies exceeding ± 1 standard deviation during the far-future period are averaged to obtain positive and negative composites, respectively.

Results from the composite analysis applied to $PO_4$ concentration, MLD and vertical diffusivity (Fig. 14a and b) indicate that the nutrient variations at the shelf break are induced by variations in vertical mixing. The main atmospheric driver for these variations can be identified as the North Atlantic Oscillation (NAO; Fig. 15). Variations are strongest though when the Iceland low anomaly dominates over the Azores high anomaly. In the following the two extreme phases of the variability are described.

During positive phases, stronger westerly winds over the NE Atlantic lead to large-scale enhanced vertical mixing via wind stirring and enhanced surface cooling. Besides, the particularly shallow Atlantic MLD in the far-future period gives way to the formation of a subpycnocline wedge of northward flowing warm and salty subtropical water attached to the shelf break (Fig. 14c). Due to the enhanced mixing during positive phases, this warm and salty water becomes eroded and thus increases the density of the upper water column (by up to 0.5 kg m$^{-3}$ in March

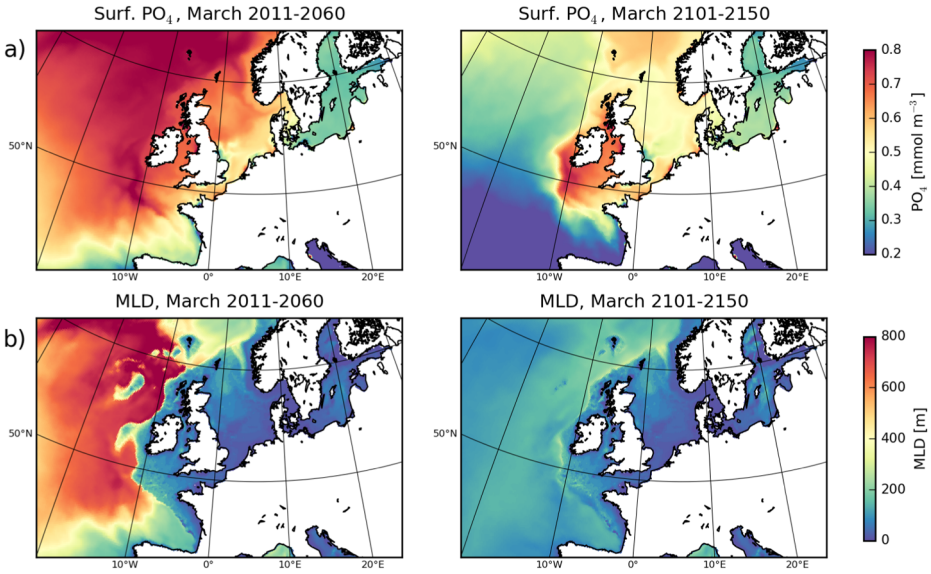


**Fig. 9.** March surface $PO_4$ concentrations (a) and MLD (b) according to scenario RCP8.5 (r1) for the near-future period 2011–2060 (left) and far-future period 2101–2150 (right).

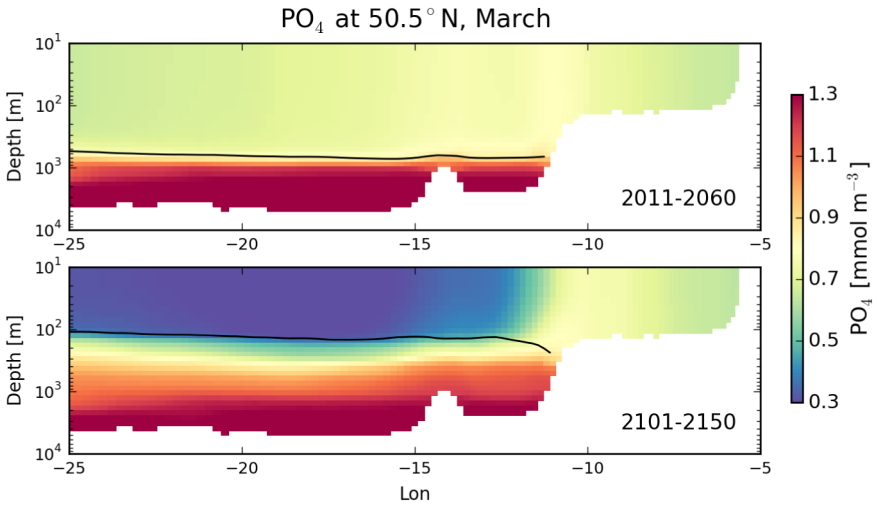


**Fig. 10.** Vertical distribution of March $PO_4$ concentrations exemplified at 50.5°N (Fig. 1, S1). Mean over the near-future period 2011–2060 (top) and far-future period 2101–2150 (bottom) of scenario RCP8.5 (r1). Black line: MLD. Note the logarithmic depth scale.

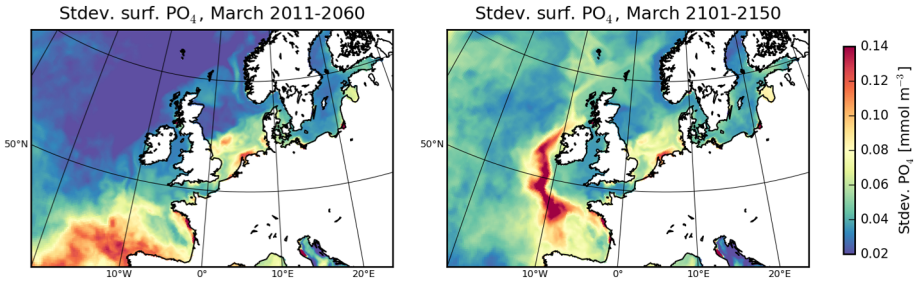


**Fig. 11.** Standard deviation of March surface $PO_4$ concentrations (detrended) according to scenario RCP8.5 (r1) for the near-future period 2011–2060 (left) and far-future period 2101–2150 (right).

compared to negative phases) and the surface heat loss to the atmosphere (by up to 50 W $m^{-2}$), initiating a positive feedback with maximum vertical velocities O(10 m $d^{-1}$). Moreover, the anomalous MLD is deeper than the shelf edge so that more internal wave energy concentrated in the pycnocline is reflected back to the ocean or dissipated at the slope, further enhancing vertical mixing near the shelf break (e.g. Legg and Adcroft, 2003; Nash et al., 2004; Hall et al., 2013). The enhanced mixing finally degenerates the stratification and leads to higher nutrient concentrations in the upper water masses which are advected to the shelf. Sediment and pore water fluxes on the shelf are negligibly small compared to ocean-shelf fluxes and therefore do not significantly contribute to the elevated nutrient concentrations on the shelf.

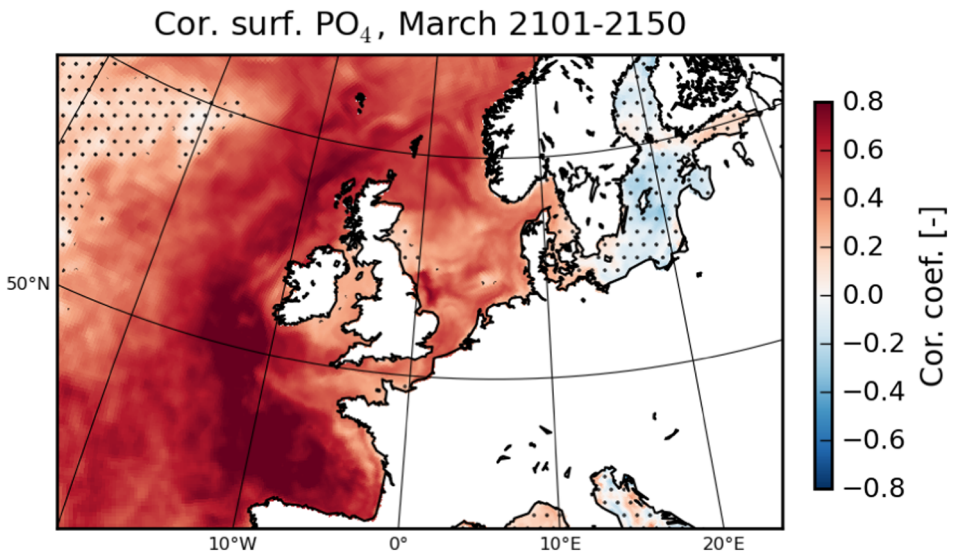


**Fig. 12.** Spatial correlation of March surface $PO_4$ variations at the Celtic Shelf break during the far-future period 2101–2150 of scenario RCP8.5 (r1). For every model grid cell, time series of $PO_4$ are correlated with the time series of $PO_4$ spatially averaged over the Celtic Shelf break region. This region is defined by standard deviations of March $PO_4$ exceeding 0.12 mmol $m^{-3}$ (Fig. 11). Dotted areas mark correlations less than 95% significance.

During negative phases, by contrast, mean westerly winds are weaker by a factor of about 2 and the horizontal internal wave energy flux is lower by about 15% with a larger energy fraction being transmitted to the shelf. Thus the vertical mixing is considerably reduced, in particular near the shelf break, where the warm and salty water at intermediate depths intensifies the vertical stratification. The reduced mixing with vertical velocities O(1 m $d^{-1}$) enables the front to propagate eastward. On the shelf, tidal currents provide enough additional energy to keep the entire water column vertically mixed (Fig. 14b), thus representing a natural boundary for the nutrient front.

This mode of variability mainly acts on interannual time scales. Nutrient anomalies are strongest at the Celtic Shelf break and decrease northward, where subsurface concentrations are considerably lower and the front is weaker. The enhanced variability, however, occurs all along the continental margin north of about 47°N (Fig. 16). A transect north of Scotland (S2 in Fig. 1) is shown in Fig. 17, exemplifying the variability in water masses flowing into the North Sea (east of about 9°W), with maximum variations at the shelf break of about 0.08 mmol P $m^{-3}$. South of 47°N, effective wind-driven exchange at the Armorican Shelf break is larger than along-slope flow (Huthnance et al., 2009), inhibiting the development of a nutrient front with enhanced variability.

### 4.3. Enhanced multidecadal variability

In addition to the mode of variability described in the previous subsection, an overlying multidecadal signal can be recognized in the time series of both nutrient concentrations along the shelf break (Fig. 13b) and primary production in the northern North Sea (Fig. 8). The NAO indeed shows similar variations on multidecadal time scales (not shown). The signal though is further amplified by variations in nutrient-rich subtropical subsurface water migrating northward at intermediate depths into the complex circulation of the eastern subpolar North Atlantic (Pollard et al., 1996; Huthnance et al., 2001). The gateway for northward intrusion of subtropical water is modulated by the strength and extension of the SPG (e.g. Hátún et al., 2005; Frankignoul et al., 2009; Burkholder and Lozier, 2011; Holliday et al., 2015) and is thus also influenced by the NAO (e.g. Lohmann et al., 2009; Sarafanov, 2009;

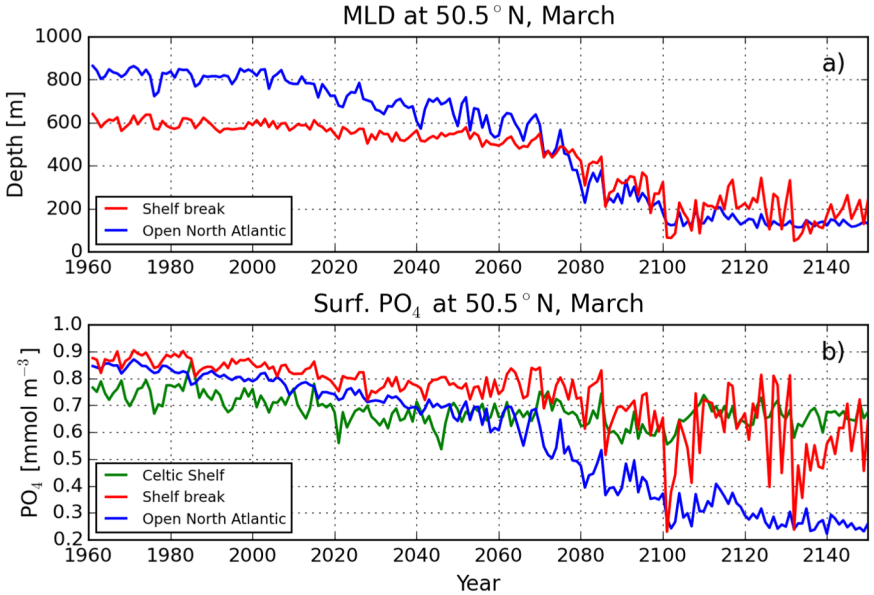


**Fig. 13.** Time series of March MLD (a) and surface $PO_4$ concentrations (b) at 50.5°N (Fig. 1, S1) for the historical period and scenario RCP8.5 (r1). Blue: Open North Atlantic (15–20°W). Red: Shelf break (10–12°W). Green: Celtic Shelf (6–8°W).

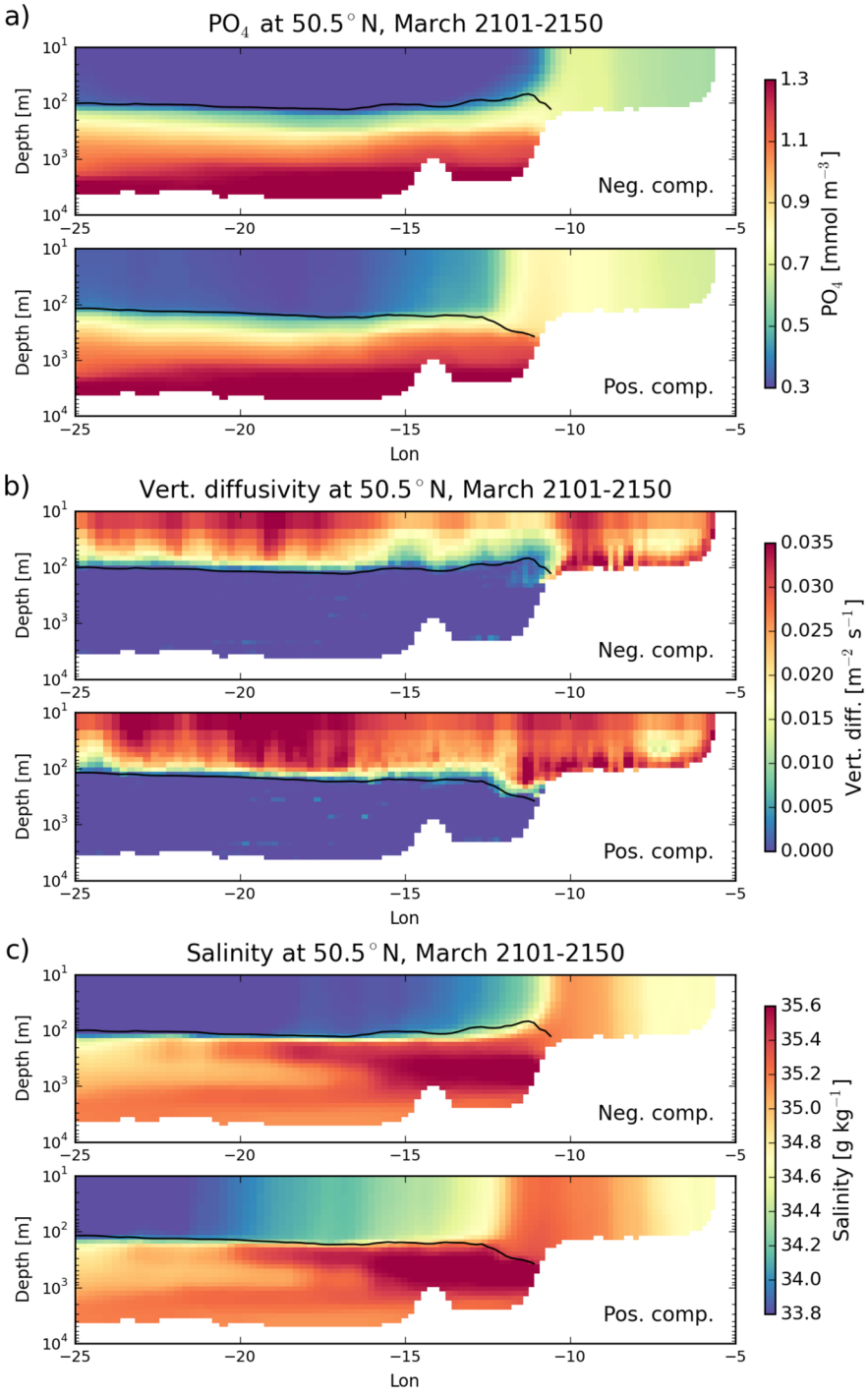


**Fig. 14.** Vertical distributions of $PO_4$ concentrations (a), vertical diffusivity as a measure of vertical mixing (b), and salinity (c) in March at 50.5°N (Fig. 1, S1). For each parameter negative (top) and positive (bottom) composites are shown, constructed from March surface $PO_4$ anomalies exceeding ± 1 standard deviation at the Celtic Shelf break during the far-future period 2101–2150 of scenario RCP8.5 (r1). Black line: MLD. Note the logarithmic depth scale.

Woollings et al., 2015). In our simulations, accordingly, related multidecadal variations are found in the SPG and MOC.

Under present-day and near-future conditions deep winter convection homogenizes the upper water column (Fig. 10). With the successive shoaling of the wintertime mixed layer in response to a warming climate, replenishment of surface nutrients from intermediate depths is weakened, leaving more nutrients in subsurface water masses (Fig. 18). During the course of the century, the shallower layers become isolated from the ocean surface. After about year 2090, mean MLDs do not exceed 200 m, which leads to higher nutrient concentrations over the entire intermediate depth range. In the far-future period, finally, remaining multidecadal variations in intermediate depth water mass properties are transferred to the shelf by ocean-shelf exchange, additionally amplifying the variability shown in Figs. 8 and 13.

### 4.4. Impact on northern North Sea primary production

We have seen that the nutrient transport from the Atlantic to the northern North Sea shows increased variability in the far future and so do pre-bloom nutrient concentrations and primary production in this

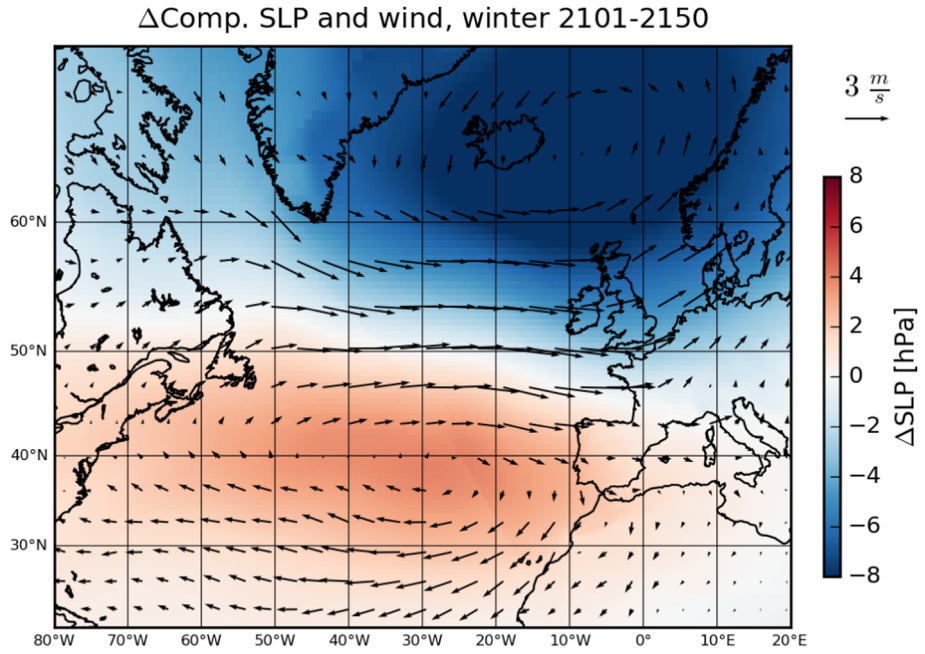


**Fig. 15.** Difference between positive and negative composites of winter (DJF) sea level pressure and near-surface wind field for pronounced $PO_4$ anomalies at the Celtic Shelf break during the period 2101–2150 of scenario RCP8.5 (r1).

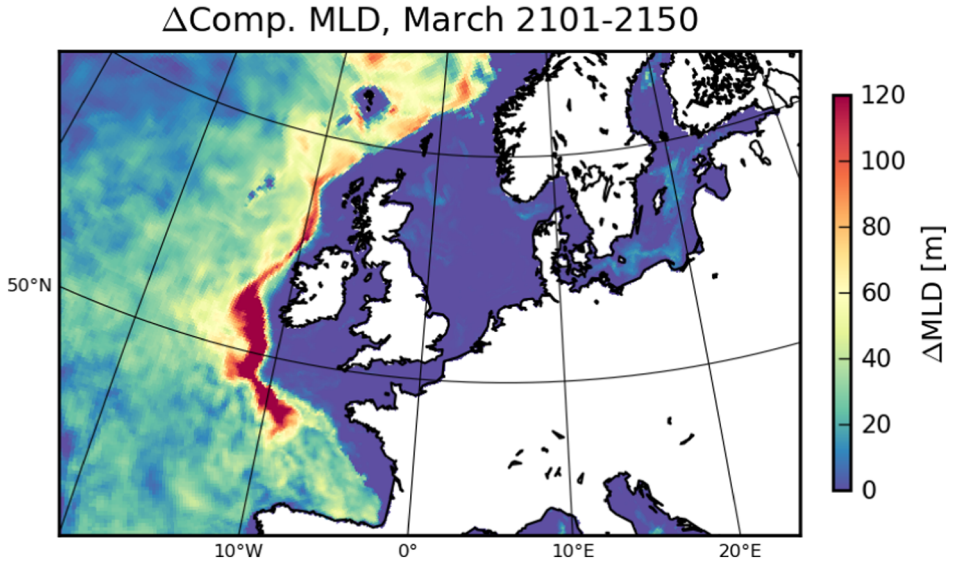


**Fig. 16.** Difference between positive and negative March MLD composites for pronounced $PO_4$ anomalies at the Celtic Shelf break during the period 2101-2150 of scenario RCP8.5 (r1).

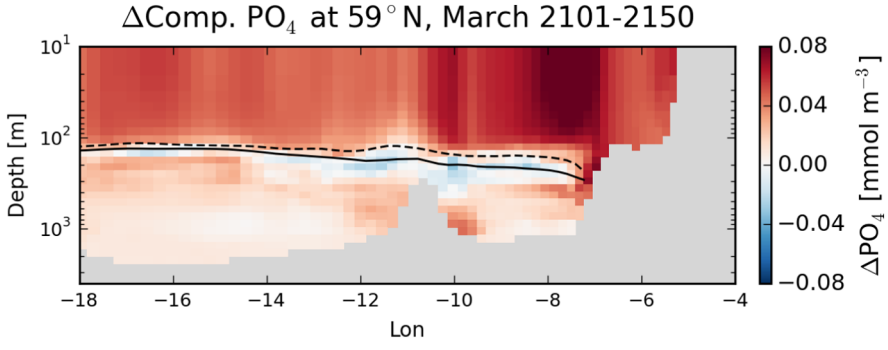


**Fig. 17.** Difference between positive and negative composites of March $PO_4$ concentrations at a transect crossing the shelf break at 59°N (Fig. 1, S2). Composites correspond to pronounced $PO_4$ anomalies at the Celtic Shelf break during the period 2101–2150 of scenario RCP8.5 (r1). Black lines: MLD of positive (solid) and negative (dashed) composites. Note the logarithmic depth scale.

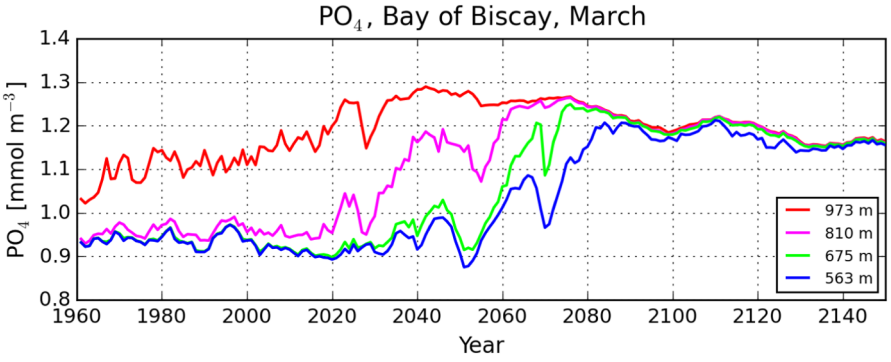


**Fig. 18.** Time series of March $PO_4$ concentrations at intermediate depths near the Bay of Biscay (Fig. 1), to the south of the high-variability region at the shelf break (Fig. 11), for the historical period and scenario RCP8.5 (r1). Given depths refer to model layers 18–21.

region. In this subsection we analyze, whether there are other relevant processes affecting the variability of primary productivity and nutrient availability. To this end we focus separately on spring bloom and summer growth and apply a correlation analysis between primary production and key physical quantities known to affect it.

Searching for the causes of variability in spring bloom production the analysis of linearly detrended time series (Table 1) points to a shift in the main governing parameters from pycnocline depth and SST for the near future to winter nutrient concentrations for the far future. This change is dominated by the strong multidecadal nutrient variations initiated by the shallow far-future MLD (Section 4.3). Applying a highpassfilter by removing 10-year running means reduces the differences between the two time periods for interannual variability. For the far future, the influence of interannually varying wintertime nutrient concentrations even weakens due to lower mean concentrations. Nevertheless, the influence of the pycnocline intensity is not affected by multidecadal nutrient variations but decreases for both detrend methods, suggesting that the future stratification might have passed a critical strength. For historical and near-future conditions, spring bloom production is obviously negatively correlated with stratification. However, there is a threshold at a vertical density gradient of approximately 50 g $m^{-4}$ (Fig. 19). Above this value, there is no clear correlation with primary production visible anymore.

Similarly, in summer, lower Atlantic nutrient import dominates the variability of far-future primary production in the northern North Sea (Table 2). Nevertheless, multidecadal variations do not outweigh other parameters to the same extent as in spring. Thus the highpass filtering does not crucially affect the correlation coefficients. The pycnocline shoals by about 3 m (compared to near future) even though wind stress does not change significantly. This indicates that in the far future the depth of the pycnocline is rather governed by temperature variations (correlation between pycnocline depth and SST increases from about −0.5 near-future to −0.6 far-future for both detrend methods). The latter do not correlate with summer phytoplankton growth due to the opposing effects of favorable growth conditions but shallower pycnoclines during positive temperature anomalies. The correlation of summer productivity with pycnocline intensity is negative for the near future and insignificant for the far future. Above a threshold of approximately 80 g $m^{-4}$ the strength of the summer stratification has no longer a negative effect on primary production (Fig. 19).

**Table 1**
Correlation coefficients between spring bloom primary production in the northern North Sea (May) and various influencing parameters (prim prod: primary production; pycno int: pycnocline intensity; pycno dep: pycnocline depth). Near-future (2011–2060) and far-future (2101–2150) periods of scenario RCP8.5 (r1) are compared for two different detrend methods. Linearly detrended time series represent anomalies of the full signal including multidecadal variations, whereas time series detrended by removing 10-year running means only retain subdecadal variations. All considered parameters approximately follow linear trends within the two periods. Bold values highlight correlations exceeding 99.5% significance. Values less than 95% significance are omitted.

| Variables | Linear detrend | | Running mean detrend | |
|---|---|---|---|---|
| | Near future | Far future | Near future | Far future |
| Prim prod - March $PO_4$ | 0.33 | **0.49** | 0.38 | 0.28 |
| Prim prod - pycno int | −0.35 | −0.29 | −0.38 | – |
| Prim prod - pycno dep | **0.64** | 0.35 | **0.62** | **0.49** |
| Prim prod - SST | **− 0.46** | −0.36 | **− 0.44** | **− 0.56** |
| Prim prod - wind stress | 0.36 | – | 0.38 | 0.32 |

### 4.5. Discussion

In our simulations for far-future RCP8.5 conditions, the shoaling of the NE Atlantic winter mixed layer to the depth of the outer NWES in combination with shelf break mixing leads to the development of a cross-shelf break nutrient front with higher concentrations on the NWES than in the open Atlantic (Fig. 10 and Fig. 20). Shelf break mixing, of course, is not a phenomenon invoked only under far-future conditions but its influence on shaping upper ocean nutrient concentrations is negligible under sufficiently deep present-day and near-future winter mixed layers.

Moreover, a buoyancy-driven positive feedback between the depth and density of the winter mixed layer enhances the NAO-driven variability in the Atlantic nutrient supply to the shelf on interannual and multidecadal scales (Fig. 20). Sporadic mixing processes due to internal tides, shelf waves, fluctuations and meandering of the slope current can be ruled out as significant causal vectors. Respective variations were measured with maximum periods O(10 d) (e.g. White and Bowyer, 1997; Sherwin et al., 2006; Simpson and McCandliss, 2013), whereas the anomalies shown in Fig. 14 develop steadily over the whole winter season. The multidecadal variability is further amplified by variations in nutrient-rich deeper water masses. Both effects peak at the Celtic Shelf break but occur all along the continental margin. Imprints on the shelf are therefore also identified in the northern North Sea. Water masses originating as far as west of Scotland are able to flush the northern North Sea within one winter season (Marsh et al., 2017).

In the subpolar North Atlantic, salinity increases with depth similar to nutrient concentrations (Fig. 14c). The decreasing MLD therefore also leads to the development of a cross-shelf break salinity front (Fig. C.23) with enhanced variability along the shelf edge and in the northern North Sea (Fig. C.24).

In scenario RCP4.5, winter MLD shoaling does not dissociate intermediate depths from surface water characteristics to the same extent. In particular, the shoaling is not strong enough for the effect of vertical mixing to establish a distinct cross-shelf break front nor to enhance interannual variations along the shelf break. In our simulations, Atlantic upper ocean nutrient concentrations drop below shelf

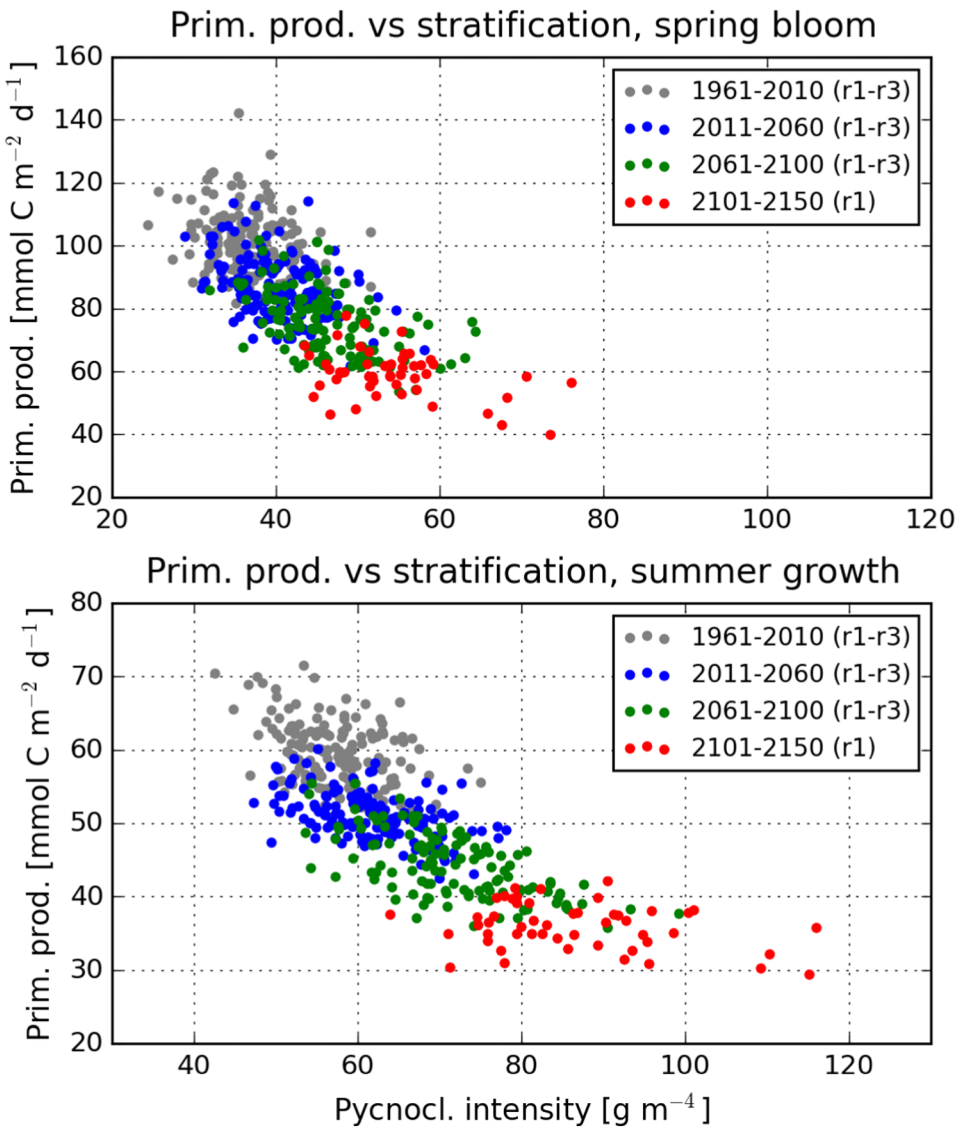


**Fig. 19.** Scatter diagrams for primary production over pycnocline intensity in the northern North Sea for the historical period and scenario RCP8.5. Top: Spring bloom (May). Bottom: Summer growth (June–August). For 1961–2100 three realizations are shown (r1–r3), for 2101–2150 only one realization is available (r1).

**Table 2**
As Table 1 but for phytoplankton summer growth in the northern North Sea (June-August).

| Variables | Linear detrend | | Running mean detrend | |
|---|---|---|---|---|
| | Near future | Far future | Near future | Far future |
| Prim prod - March $PO_4$ | **0.45** | **0.84** | **0.48** | **0.79** |
| Prim prod - pycno int | **− 0.46** | – | **− 0.52** | – |
| Prim prod - pycno dep | **0.60** | 0.31 | **0.60** | 0.37 |
| Prim prod - SST | – | – | – | – |
| Prim prod - wind stress | **0.56** | – | **0.49** | – |

concentrations when winter MLDs off the Celtic Shelf become shallower than about 600 m, which is reached around the 2060s for scenario RCP8.5 (Fig. 13) but sets in just at the end of the century for RCP4.5. In the latter scenario, MLD beyond the year 2100 does not change much further (not shown) because atmospheric greenhouse gas concentrations ultimately level off around the year 2110. Atlantic nutrient concentrations at intermediate depths show a continuous decline without significant multidecadal variations during the far-future period of this particular RCP4.5 realization (not shown). The steady nutrient decline drives a steady weakening in northern North Sea primary production (Fig. 8). Periods of stationarity, steady changes and multidecadal variations in sub-mixed layer conditions are found in virtually all simulations of both the downscaling regional and forcing global model systems. Hence, the closeness between the productivities at the end of the RCP4.5 and RCP8.5 simulations (Fig. 8) has to be interpreted with care since it is influenced by natural variability.

The future development of a cross-shelf break nutrient front mainly depends on the projected shoaling of the MLD and on-shelf nutrient transport. An additional influence might result from sediment resuspension on the shelf, limiting deposition of organic matter. Although the resuspension scheme in our model yields reasonable present-day deposition rates (Section 2.3), further uncertainties are related to the individual sediment constituents and respective grain sizes and densities. Riverine nutrient loads are of minor importance, except for the southern North Sea. Even under far-future conditions the largest fraction of the total nutrient supply to the NWES by far originates from the Atlantic (about 96%).

Accordingly, in the parent RCP8.5 simulation by MPI-ESM a nutrient front at the continental margin with enhanced variability does not develop (Fig. 21). Typical for global circulation models, MPI-ESM underestimates MLDs, ignores tidal waves and sediment resuspension, and simulates substantially weaker slope currents and cross-shelf break

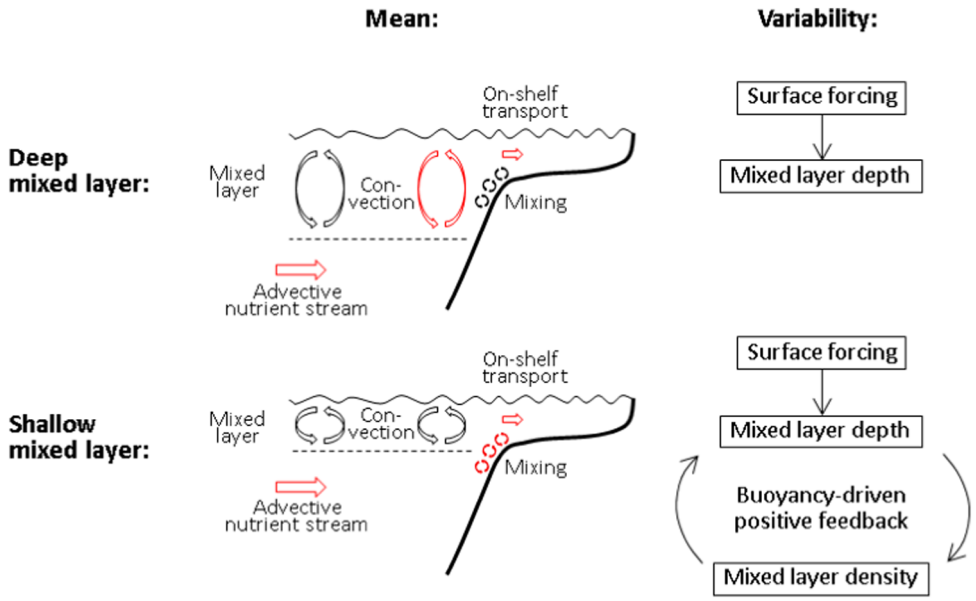


**Fig. 20.** Schematic process chain of North Atlantic nutrient supply to the NWES for deep (top) and shallow (bottom) winter mixed layers. Left: Mean state. Red parts mark the nutrient pathway from intermediate depths to the shelf. Right: Driving mechanism for interannual and multidecadal variability.

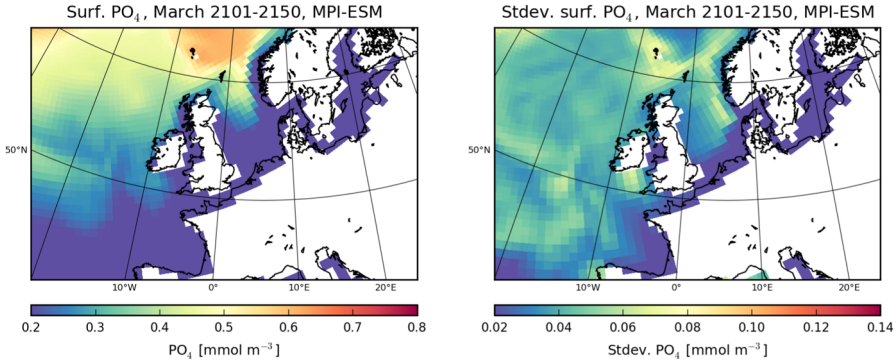


**Fig. 21.** March surface $PO_4$ concentration according to scenario RCP8.5 (r1) for the far-future period 2101–2150, simulated by the parent earth system model MPI-ESM. Mean (left) and standard deviation (right). Compare with Fig. 9a and Fig. 11, respectively.

exchange (e.g. Sallée et al., 2013; Huang et al., 2014). In particular cross-shelf break transport is attributable to ageostrophy (Huthnance, 1995), requiring meso-scale grid resolution. For downscaling experiments with conventional regional ocean models, we therefore highly recommend to include the shelf break into the model domain to capture such regime shifts properly. Furthermore, since the transition to the new regime already starts within the last decades of the 21st century, we highly recommend to run the simulations some decades into the 22nd century.

In the northern North Sea, the strengthening of the seasonal stratification weakens the primary production during the 21st century in addition to the reduced nutrient import from the North Atlantic, as also indicated for scenario A1B in Holt et al. (2012, 2016). After the year 2100, however, the strength of the stratification in scenario RCP8.5 effectively blocks vertical nutrient fluxes and hence passes a threshold for influencing primary production. In scenario RCP4.5 this threshold is not reached, leaving seasonal stratification a significant causal influence also in the far-future period.

In both scenarios NE Atlantic winter MLDs stabilize in the 22nd century. Besides, in open shelf areas an increasing influence of winter nutrient concentrations on primary production is indicated in Table 1. It can be expected that NWES primary production beyond the year 2150 continues to be strongly influenced by Atlantic nutrient concentrations at intermediate depths. In the control simulation, however, Atlantic sub-mixed layer nutrient concentrations show a negative drift (Section 2.2), also recognizable in Fig. 6a and in Fig. 18 after the year 2080. The quantification of the influence of model drift beyond 2150 would thus require new control simulations for the new shallow MLD states. We therefore have not extended our simulations further.

## 5. Conclusions

Our ensemble simulations for emission scenarios RCP4.5 and RCP8.5 have shown that during the 21st century, long-term trends of Atlantic nutrient supply to the NWES are generally governed by decreasing NE Atlantic winter MLDs. Reduced winter MLDs limit the nutrient transport from intermediate depths to the upper ocean and hence the nutrient import from the open ocean to the shelf. The decreasing Atlantic nutrient import drives a continuous decline in biological productivity and atmospheric $CO_2$ uptake in open shelf areas. In the northern North Sea there is an additional influence due to a strengthening of the seasonal stratification.

From the ensemble spread of our simulations we have estimated that for the projected productivity changes the uncertainty due to internal variability of the forcing global model is smaller than the uncertainty due to the choices of the global model and the downscaling regional model. Comparatively low internal variability is associated with changes in SST and seasonal stratification on the shelf as well as Atlantic MLD and upper-ocean nutrient concentrations near the shelf

break. Higher internal variability is indicated for changes in Atlantic sub-mixed layer nutrient concentrations and the intensity of the SPG, increasing the uncertainties in Atlantic MLD changes and upper-ocean nutrient concentrations further west of the shelf break.

In scenario RCP8.5, both the shoaling of the NE Atlantic winter MLD and the stratification strengthening on the shelf pass critical values by the end of the century and invoke a regime shift in the dynamics of Atlantic nutrient supply. The exceptionally shallow Atlantic MLD leads to exceptionally low upper ocean nutrient concentrations. Along the continental margin, however, vertical mixing processes at the shelf break maintain a continuous transport of nutrient-enriched sub-pycnocline water masses to the shelf. Owing to this mechanism, the nutrient supply to the shelf becomes decoupled from upper ocean nutrient concentrations in the adjacent North Atlantic. The sustained nutrient transport to the shelf causes a reversal of the ratio between NE Atlantic and NWES surface nutrient concentrations and initiates the formation of an ocean-shelf nutrient front. As a consequence, the projected weakening in NWES primary production is less pronounced than it would be expected from declining nutrient concentrations in the upper NE Atlantic. Moreover, a buoyancy-driven positive feedback between winter convection and NAO-induced variations in MLD enhances the variability of on-shelf nutrient fluxes on interannual and multidecadal scales, affecting the variability of primary production in open shelf areas. The multidecadal variability is further enhanced by multidecadal variations in Atlantic subpycnocline nutrient concentrations. The latter are naturally influenced by centennial and even millennial variations of the large-scale North Atlantic circulation, making future projections for the NWES beyond the year 2100 particularly challenging.

Independent of the considered scenarios, our results suggest that under a warming climate ocean-shelf exchange potentially exerts growing influence on the NWES ecosystem. Since the driving mechanism for this is Atlantic MLD shoaling, a similar tendency is indicated for other biologically rich shelf seas with marked cross-shelf break transports and deep present-day MLDs off the shelf, such as the Faroe Shelf, Iceland Shelf and East Greenland Shelf.

Our model system does not include any species distribution or stock assessment models to explore impacts on higher trophic levels. Nevertheless, there is observational evidence that fluctuations in marine plankton resulted in long-term changes in NWES fish recruitment (e.g. Beaugrand et al., 2003; Kirby et al., 2007; Alheit et al., 2012; Nicolas et al., 2014). In particular, species with short, plankton-based food chains responded dramatically and quickly to changes in environmental conditions (e.g. Lehodey et al., 2006; Checkley et al., 2009). Distributional shifts of plankton groups as well as changes in growth rates led to altered community structures and diversity patterns (e.g. Doney et al., 2012). In a recent study, low-frequency variations in primary production have been linked to whole regime shifts in the ecosystem (Daewel and Schrum, 2017). The projected high variability in primary production thus potentially destabilizes species abundance, distribution and migration at higher trophic levels via bottom-up control and may hinder adaptation of the NWES ecosystem to the new ocean climate.

## Acknowledgment

This work contributed to the BMBF-funded joint research project RACE - Regional Atlantic Circulation and Global Change (grant 03F0729D) and the EU-funded collaborative project PEARL - Preparing for extreme and rare events in coastal regions (grant 603663 under the 7th Framework Programme for Research and Innovation). Computational resources were made available by the German Climate Computing Center (DKRZ) through the support from the German Federal Ministry of Education and Research (BMBF).

## Appendix A. Sediment resuspension

The implementation of sediment resuspension in HAMOCC is derived from Wilcock (2004). Solid sediment constituents become resuspended when a critical bottom shear stress $\tau_c$ is exceeded. The latter is determined by the density and grain size of the sediment and the effect of fluid viscosity on grain movement.

$$\tau_c = \tau_c^* \left( \frac{\rho_s}{\rho_w} - 1 \right) \rho_w g D \tag{A.1}$$

with the dimensionless critical shear stress $\tau_c^*$, the mean density of the uppermost sediment layer $\rho_s$, the density of the near-bottom water $\rho_w$, the gravitational acceleration $g$, and the mean grain size of the uppermost sediment layer $D$. The value of $\tau_c^*$ is represented by the Shields curve, following the function

$$\tau_c^* = 0.105(S^*)^{-0.3} + 0.045\ exp(-35(S^*)^{-0.59}) \tag{A.2}$$

with the dimensionless viscosity $S^*$ being

$$S^* = \frac{\sqrt{\left( \frac{\rho_s}{\rho_w} - 1 \right) g D^3}}{\nu} \tag{A.3}$$

with the kinematic viscosity of the near-bottom water $\nu$. The actual bottom shear stress $\tau$ is calculated from the near-bottom flow speed and the sediment drag coefficient in dependence on the mean grain size.

$$\tau = \rho_w c_D u^2 \tag{A.4}$$

with the sediment drag coefficient $c_D$ and the near-bottom flow speed $u$.

$$c_D = 0.16 \left( 1 + ln \frac{D}{12h} \right)^{-2} \tag{A.5}$$

with the bottom layer thickness $h$. Whenever $\tau$ is greater than $\tau_c$ sediment becomes eroded. The rate of erosion $q_s$ is determined by the sediment density and the amount by which $\tau_c$ is exceeded.

$$q_s = \frac{8}{\left( \frac{\rho_s}{\rho_w} - 1 \right) g} \left( \frac{\tau - \tau_c}{\rho_w} \right)^{\frac{3}{2}} \tag{A.6}$$

## Appendix B. Projected changes in $CO_2$ uptake

The North Sea region has been identified as a net sink for atmospheric $CO_2$ of about 1.3–1.4 mol C $m^{-2} yr^{-1}$ (e.g. Thomas et al., 2005; Thomas et al., 2010; Kühn et al., 2010; Laruelle et al., 2014), though uncertainties associated with estimated spatio-temporal means are still large (Gruber, 2015). Dissolved inorganic carbon sequestered by phytoplankton growth is exported below the seasonal pycnocline and advected out of the North Sea to the deep ocean, inducing atmospheric carbon drawdown at the sea surface. Simulated present-day $CO_2$ uptake in the North Sea ranges between 1.5 and 1.6 mol C $m^{-2} yr^{-1}$, reflecting an overestimation of about 15%.

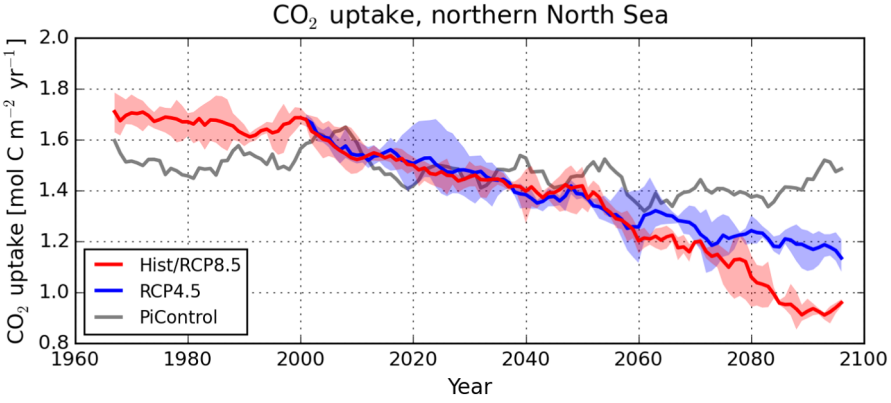


**Fig. B.22.** Time series (10-year running means) of northern North Sea atmospheric $CO_2$ uptake. Gray line: preindustrial control; blue line: ensemble mean RCP4.5; red line: ensemble mean historical and RCP8.5; shaded areas: ensemble spread between minimum and maximum values.

Future changes in $CO_2$ uptake are determined by the balance between weakening influences such as less primary production and higher water temperature reducing $CO_2$ solubility, and enhancing influences such as increased atmospheric $CO_2$ partial pressure ($pCO_2$), lower salinity enhancing $CO_2$ solubility, and stronger stratification inhibiting subpycnocline respiratory $CO_2$ release to escape to the atmosphere. Moreover, air-sea $CO_2$ exchange becomes generally more sensitive in the future because of the lower buffer capacity of the ocean at higher $pCO_2$.

In the northern North Sea, changes in temperature and salinity result in a lower $CO_2$ solubility of the sea water by 3% for RCP4.5 and 6% for RCP8.5. By ignoring nonlinearities of the system, we can estimate that for RCP4.5 the decreasing rate of atmospheric $pCO_2$ rise during the second half of the 21st century results in a weakening in $CO_2$ uptake by less than 0.05 mol C $m^{-2} yr^{-1}$, while for RCP8.5 the ever increasing rate of atmospheric $pCO_2$ rise increases $CO_2$ uptake by about 0.2 mol C $m^{-2} yr^{-1}$. As shown in Fig. B.22, total $CO_2$ uptake in the northern North Sea is reduced by about 0.4 mol C $m^{-2} yr^{-1}$ (24%) for scenario RCP4.5 and 0.6 mol C $m^{-2} yr^{-1}$ (36%) for RCP8.5 (0.1 mol C $m^{-2} yr^{-1}$ ensemble spread). Thus, for RCP4.5 the drop in total $CO_2$ uptake can be mainly attributed to changes in primary production, stratification and net carbon export, including related changes in ocean alkalinity. For RCP8.5 these components cause a drop of about 0.8 mol C $m^{-2} yr^{-1}$ (0.6 + 0.2), compensating for the increasing rate of atmospheric $pCO_2$ rise. Dissolution of calcium carbonate is not relevant during the 21st century since the surface water in the northern North Sea remains supersaturated with respect to carbonate ion.

## Appendix C. Supplementary data

Supplementary data to this article can be found online at https://doi.org/10.1016/j.jmarsys.2018.10.002.

## References


Ådlandsvik, B., 2008. Marine downscaling of a future climate scenario for the North Sea. Tellus A 60 (3), 451–458.

Alexander, M.A., Scott, J.D., Friedland, K.D., Mills, K.E., Nye, J.A., Pershing, A.J., Thomas, A.C., 2018. Projected sea surface temperatures over the 21st century: changes in the mean, variability and extremes for large marine ecosystem regions of Northern Oceans. Elem. Sci. Anth. 6 (9), 25.

Alheit, J., Pohlmann, T., Casini, M., Greve, W., Hinrichs, R., Mathis, M., O'Driscoll, K., Vorberg, R., Wagner, C., 2012. Climate variability drives anchovies and sardines into the North and Baltic Seas. Prog. Oceanogr. 96 (1), 128–139.

Beaugrand, G., Brander, K.M., Alistair, L.J., Souissi, S., Reid, P.C., 2003. Plankton effect on cod recruitment in the North Sea. Nature 426, 661–664.

Bopp, L., Monfray, P., Aumont, O., Dufresne, J.L., Treut, H.L., Madec, G., Terray, L., Orr, J.C., 2001. Potential impact of climate change on marine export production. Glob. Biogeochem. Cycles 15 (1), 81–99.

Bopp, L., Resplandy, L., Orr, J.C., Doney, S.C., Dunne, J.P., Gehlen, M., Halloran, P., Heinze, C., Ilyina, T., Séférian, R., Tjiputra, J., Vichi, M., 2013. Multiple stressors of ocean ecosystems in the 21st century: projections with CMIP5 models. Biogeosciences 10, 6225–6245.

Brion, N., Baeyens, W., De Galan, S., Elskens, M., Laane, R.W.P.M., 2004. The North Sea: source or sink for nitrogen and phosphorus to the Atlantic Ocean? Biogeochemistry 68 (3), 277–296.

Bülow, K., Dieterich, C., Elizalde, A., Gröger, M., Heinrich, H., Hüttl-Kabus, S., Klein, B., Mayer, B., Meier, H.E.M., Mikolajewicz, U., Narayan, N., Pohlmann, T., Rosenhagen, G., Schimanke, S., Sein, D., Su, J., 2014. Comparison of 3 coupled models in the North Sea region under todays and future climate conditions. Bundesanstalt für Gewässerkunde, Koblenz. KLIWAS Schriftenreihe 27, 270.

Burkholder, K.C., Lozier, M.S., 2011. Mid-depth Lagrangian pathways in the North Atlantic and their impact on the salinity of the eastern subpolar gyre. Deep-Sea Res. I Oceanogr. Res. Pap. 58 (12), 1196–1204.

Capuzzo, E., Lynam, C.P., Barry, J., Stephens, D., Forster, R.M., Greenwood, N., McQuatters-Gollop, A., Silva, T., van Leeuwen, S.M., Engelhard, G.H., 2018. A decline in primary production in the North Sea over 25 years, associated with reductions in zooplankton abundance and fish stock recruitment. Glob. Chang. Biol. 24, 352–364.

Checkley, D., Alheit, J., Oozeki, Y., Roy, C. (Eds.), 2009. Climate Change and Small Pelagic Fish. Cambridge University Press, Cambridge, U.K., pp. 372.

Chust, G., Allen, J.I., Bopp, L., Schrum, C., Holt, J., Tsiaras, K., Zavatarelli, M., Chifflet, M., Cannaby, H., Dadou, I., Daewel, U., Wakelin, S.L., Machu, E., Pushpadas, D., Butenschon, M., Artioli, Y., Petihakis, G., Smith, C., Garçon, V., Goubanova, K., Vu, B.L., Fach, B.A., Salihoglu, B., Clementi, E., Irigoien, X., 2014. Biomass changes and trophic amplification of plankton in a warmer ocean. Glob. Chang. Biol. 20 (7), 2124–2139.

Daewel, U., Schrum, C., 2017. Low-frequency variability in North Sea and Baltic Sea identified through simulations with the 3-D coupled physical-biogeochemical model ECOSMO. Earth Syst. Dynam. 8, 801–815.

De Haas, H., Van Weering, T.C.E., De Stigter, H., 2002. Organic carbon in shelf seas: sinks or sources, processes and products. Cont. Shelf Res. 22, 691–717.

Doney, S.C., Ruckelshaus, M., Duffy, J.E., Barry, J.P., Chan, F., English, C.A., Galindo, H.M., Grebmeier, J.M., Hollowed, A.B., Knowlton, N., Polovina, J., Rabalais, N.N., Sydeman, W.J., Talley, L.D., 2012. Climate change impacts on marine ecosystems. Annu. Rev. Mar. Sci. 4, 11–37.

Elizalde Arellano, A., 2011. The Water Cycle in the Mediterranean Region and the Impacts of Climate Change. PhD thesis. Reports on Earth System Science. Max-

Planck-Institute for Meteorology, Hamburg, Germany, pp. 128.
Frankignoul, C., Deshayes, J., Curry, R., 2009. The role of salinity in the decadal variability of the North Atlantic meridional overturning circulation. Clim. Dyn. 33, 777–793.
Fu, W., Randerson, J.T., Moore, J.K., 2016. Climate change impacts on net primary production (NPP) and export production (EP) regulated by increasing stratification and phytoplankton community structure in the CMIP5 models. Biogeosciences 13 (18), 5151–5170.
Giorgetta, M.A., Jungclaus, J., Reick, C.H., Legutke, S., Bader, J., Böttinger, M., Brovkin, V., Crueger, T., Esch, M., Fieg, K., Glushak, K., Gayler, V., Haak, H., Hollweg, H.D., Ilyina, T., Kinne, S., Kornblueh, L., Matei, D., Mauritsen, T., Mikolajewicz, U., Mueller, W., Notz, D., Pithan, F., Raddatz, T., Rast, S., Redler, R., Roeckner, E., Schmidt, H., Schnur, R., Segschneider, J., Six, K.D., Stockhause, M., Timmreck, C., Wegner, J., Widmann, H., Wieners, K.H., Claussen, M., Marotzke, J., Stevens, B., 2013. Climate and carbon cycle changes from 1850 to 2100 in MPI-ESM simulations for the Coupled Model Intercomparison Project phase 5. J. Adv. Model. Earth Syst. 5 (3), 572–597.
Gouretski, V.V., Koltermann, K.P., 2004. WOCE global hydrographic climatology. Bundesamt für Seeschifffahrt und Hydrographie, Hamburg und Rostock. Berichte des Bundesamtes für Seeschifffahrt und Hydrographie 35, 52.
Gröger, M., Maier-Reimer, E., Mikolajewicz, U., Moll, A., Sein, D., 2013. NW European shelf under climate warming: implications for open ocean - shelf exchange, primary production, and carbon absorption. Biogeosciences 10, 3767–3792.
Gruber, N., 2015. Ocean biogeochemistry: carbon at the coastal interface. Nature 517 (7533), 148–149.
Hagemann, S., Dümenil-Gates, L., 2001. Validation of the hydrological cycle of ECMWF and NCEP reanalyses using the MPI hydrological discharge model. J. Geophys. Res.-Atmos. 106, 1503–1510.
Häkkinen, S., Rhines, P.B., Worthen, D.L., 2013. Northern North Atlantic sea surface height and ocean heat content variability. J. Geophys. Res. 118 (7), 3670–3678.
Hall, R.A., Huthnance, J.M., Williams, R.G., 2013. Internal wave reflection on shelf slopes with depth-varying stratification. J. Phys. Oceanogr. 43, 248–258.
Hátún, H., Azetsu-Scott, K., Somavilla, R., Rey, F., Johnson, C., Mathis, M., Mikolajewicz, U., Coupel, P., Tremblay, J.É., Hartman, S., Pacariz, S.V., Salter, I., Ólafsson, J., 2017. The subpolar gyre regulates silicate concentrations in the North Atlantic. Sci. Rep. 7 (14576), 9.
Hátún, H., Sandø, A.B., Drange, H., Hansen, B., Valdimarsson, H., 2005. Influence of the Atlantic subpolar gyre on the thermohaline circulation. Science 309 (5742), 1841–1844.
Heinze, C., Maier-Reimer, E., Winguth, A.M.E., Archer, D., 1999. A global oceanic sediment model for long-term climate studies. Global Biogeochem. Cycles 13, 221–250.
Hjøllo, S.S., Skogen, M.D., Svendsen, E., 2009. Exploring currents and heat within the North Sea using a numerical model. J. Mar. Syst. 78 (1), 180–192.
Holliday, N.P., 2003. Air-sea interaction and circulation changes in the northeast Atlantic. J. Geophys. Res. 108 (C8), 11.
Holliday, N.P., Cunningham, S.A., Johnson, C., Gary, S.F., Griffiths, C., Read, J.F., Sherwin, T., 2015. Multidecadal variability of potential temperature, salinity, and transport in the eastern subpolar North Atlantic. J. Geophys. Res. Oceans 120, 5945–5967.
Holt, J., Butenschön, M., Wakelin, S.L., Artioli, Y., Allen, J.I., 2012. Oceanic controls on the primary production of the northwest European continental shelf: model experiments under recent past conditions and a potential future scenario. Biogeosciences 9 (1), 97–117.
Holt, J., Schrum, C., Cannaby, H., Daewel, U., Allen, I., Artioli, Y., Bopp, L., Butenschon, M., Fach, B.A., Harle, J., Pushpadas, D., Salihoglu, B., Wakelin, S., 2016. Potential impacts of climate change on the primary production of regional seas: a comparative analysis of five European seas. Prog. Oceanogr. 140, 91–115.
Holt, J., Wakelin, S., Huthnance, J., 2009. Down-welling circulation of the northwest European continental shelf: a driving mechanism for the continental shelf carbon pump. Geophys. Res. Lett. 36 (14), L14602.
Holt, J., Wakelin, S., Lowe, J., Tinker, J., 2010. The potential impacts of climate change on the hydrography of the northwest European continental shelf. Prog. Oceanogr. 86, 361–379.
Huang, C.J., Qiao, F., Dai, D., 2014. Evaluating CMIP5 simulations of mixed layer depth during summer. J. Geophys. Res. Oceans 119 (4), 2568–2582.
Huthnance, J.M., 1981. Waves and currents near the continental shelf edge. Prog. Oceanogr. 10 (4), 193–226.
Huthnance, J.M., 1986. The Rockall slope current and shelf-edge processes. Proc. Roy. Soc. Edinb. 88 (B), 83–101.
Huthnance, J.M., 1995. Circulation, exchange and water masses at the ocean margin: the role of physical processes at the shelf edge. Prog. Oceanogr. 35 (4), 353–431.
Huthnance, J.M., Coelho, H., Griffiths, C.R., Knight, P.J., Rees, A.P., Sinha, B., Vangriesheim, A., White, M., Chatwin, P.G., 2001. Physical structures, advection and mixing in the region of Goban spur. Deep-Sea Res. 48 (14), 2979–3021.
Huthnance, J.M., Holt, J.T., Wakelin, S.L., 2009. Deep ocean exchange with west-European shelf seas. Ocean Sci. 5, 621–634.
Ilyina, T., Six, K.D., Segschneider, J., Maier-Reimer, E., Li, H., Núñez-Riboni, I., 2013. The global ocean biogeochemistry model HAMOCC: model architecture and performance as component of the MPI-earth system model in different CMIP5 experimental realizations. J. Adv. Model. Earth Syst. 5, 287–315.
Jacob, D., Podzun, R., 1997. Sensitivity studies with the regional climate model REMO. Meteorog. Atmos. Phys. 63, 119–129.
Jacob, D., van den Hurk, B.J.J.M., Andræ, U., Elgered, G., Fortelius, C., Graham, L.P., Jackson, S.D., Karstens, U., Köpken, C., Lindau, R., Podzun, R., Rockel, B., Rubel, F., Sass, B.H., Smith, R.N.B., Yang, X., 2001. A comprehensive model inter-comparison study investigating the water budget during the BALTEX-PIDCAP period. Meteorog. Atmos. Phys. 77, 19–43.
Johnson, C., Inall, M., Häkkinen, S., 2013. Declining nutrient concentrations in the northeast Atlantic as a result of a weakening Subpolar Gyre. Deep-Sea Res. 82, 95–107.
Jungclaus, J., Fischer, N., Haak, H., Lohmann, K., Marotzke, J., Matei, D., Mikolajewicz, U., Notz, D., von Storch, J.S., 2013. Characteristics of the ocean simulations in MPIOM, the ocean component of the MPI earth system model. J. Adv. Model. Earth Syst. 5, 422–446.
Kirby, R.R., Beaugrand, G., Lindley, J.A., Richardson, A.J., Edwards, M., Reid, P.C., 2007. Climate effects and benthic-pelagic coupling in the North Sea. Mar. Ecol. Prog. Ser. 330, 31–38.
Kloster, S., Feichter, J., Maier-Reimer, E., Six, K.D., Stier, P., Wetzel, P., 2006. DMS cycle in the marine ocean-atmosphere system - a global model study. Biogeosciences 3, 29–51.
Kotlarski, S., Keuler, K., Christensen, O.B., Colette, A., Déqué, M., Gobiet, A., Goergen, K., Jacob, D., Lüthi, D., van Meijgaard, E., Nikulin, G., Schär, C., Teichmann, C., Vautard, R., Warrach-Sagi, K., Wulfmeyer, V., 2014. Regional climate modeling on European scales: a joint standard evaluation of the EURO-CORDEX RCM ensemble. Geosci. Model Dev. 7, 1297–1333.
Kühn, W., Pätsch, J., Thomas, H., Borges, A.V., Schiettecatte, L.-S., Bozec, Y., Prowe, A.E.F., 2010. Nitrogen and carbon cycling in the North Sea and exchange with the North Atlantic - a model study, Part II: carbon budget and fluxes. Cont. Shelf Res. 30, 1701–1716.
Laruelle, G.G., Lauerwald, R., Pfeil, B., Regnier, P., 2014. Regionalized global budget of the $CO_2$ exchange at the air-water interface in continental shelf seas. Glob. Biogeochem. Cycles 28 (11), 1199–1214.
Legg, S., Adcroft, A., 2003. Internal wave breaking an concave and convex continental slopes. J. Phys. Oceanogr. 33, 2224–2246.
Lehodey, P., Alheit, J., Barange, M., Baumgartner, T., Beaugrand, G., Drinkwater, K., Fromentin, J.M., Hare, S.R., Ottersen, G., Perry, R.I., Roy, C., van der Lingen, C.D., Werner, F., 2006. Climate variability, fish, and fisheries. J. Clim. 19, 5009–5030.
Lohmann, K., Drange, H., Bentsen, M., 2009. Response of the North Atlantic subpolar gyre to persistent North Atlantic oscillation like forcing. Clim. Dyn. 32, 273–285.
Ludwig, W., Dumont, E., Meybeck, M., Heussner, S., 2009. River discharges of water and nutrients to the Mediterranean and Black Sea: major drivers for ecosystem changes during past and future decades? Prog. Oceanogr. 80, 199–217.
Luff, R., Moll, A., 2004. Seasonal dynamics of the North Sea sediments using a three-dimensional coupled sediment-water model system. Cont. Shelf Res. 24 (10), 1099–1127.
Mahowald, N., Yoshioka, M., Collins, W., Conley, A., Fillmore, D., Coleman, D., 2006. Climate response and radiative forcing from mineral aerosols during the last glacial maximum, pre-industrial, current and doubled-carbon dioxide climates. Geophys. Res. Lett. 33 (20), L20705.
Maier-Reimer, E., 1997. Design of a closed boundary regional model of the Arctic Ocean. Workshop on polar processes in global climate, 13–15 Nov, 1996. Bull. Amer. Meteor. Soc.: 72–73.
Maier-Reimer, E., Kriest, I., Segschneider, J., Wetzel, P., 2005. The Hamburg ocean carbon cycle model HAMOCC5.1 - technical description release 1.1. Max Planck Institute for Meteorology, Hamburg, Germany. Berichte zur Erdsystemforschung 14, 50.
Marsh, R., Haigh, I.D., Cunningham, S.A., Inall, M.E., Porter, M., Moat, B.I., 2017. Large-scale forcing of the European Slope Current and associated inflows to the North Sea. Ocean Sci. 13, 315–335.
Marsland, S.J., Haak, H., Jungclaus, J.H., Latif, M., Roeske, F., 2003. The Max-Planck-Institute global ocean/sea ice model with orthogonal curvilinear coordinates. Ocean Model. 5, 91–127.
Mathis, M., Elizalde, A., Mikolajewicz, U., 2018. Which complexity of regional climate system models is essential for downscaling anthropogenic climate change in the Northwest European Shelf? Clim. Dyn. 50, 2637–2659.
Mathis, M., Elizalde, A., Mikolajewicz, U., Pohlmann, T., 2015. Variability patterns of the general circulation and sea water temperature in the North Sea. Prog. Oceanog. 135, 91–112.
Mathis, M., Pohlmann, T., 2014. Projection of physical conditions in the North Sea for the 21st century. Clim. Res. 61, 1–17.
Mikolajewicz, U., Sein, D.V., Jacob, D., Kahl, T., Podzun, R., Semmler, T., 2005. Simulating Arctic sea ice variability with a coupled regional atmosphere-ocean-sea ice model. Meteorol. Z. 14 (6), 793–800.
Moll, A., 1998. Regional distribution of primary production in the North Sea simulated by a three-dimensional model. J. Mar. Syst. 16, 151–170.
Monterey, G., Levitus, S., 1997. Seasonal variability of mixed layer depth for the world ocean, NOAA Atlas NESDIS 14. Natl. Oceanic and Atmos. Admin., Silver Spring, Md. 100.
Nash, J.D., Kunze, E., Toole, J.M., Schmitt, R.W., 2004. Internal tide reflection and turbulent mixing on the continental slope. J. Phys. Oceanogr. 34, 1117–1134.
Nicolas, D., Rochette, S., Llope, M., Licandro, P., 2014. Spatio-temporal variability of the north sea cod recruitment in relation to temperature and zooplankton. PLoS ONE 9 (2), e88447.
Pacanowski, R.C., Philander, S.G.H., 1981. Parameterization of vertical mixing in numerical models of tropical oceans. J. Phys. Ocean. 11, 1443–1451.
Pätsch, J., Burchard, H., Dieterich, C., Gräwe, U., Gröger, M., Mathis, M., Kapitza, H., Bersch, M., Moll, A., Pohlmann, T., Su, J., Ho-Hagemann, H.T.M., Schulz, A., Elizalde, A., Eden, C., 2017. An evaluation of the North Sea circulation in global and regional models relevant for ecosystem simulations. Ocean Model. 116, 70–95.
Pätsch, J., Lenhart, H., 2004. Daily loads of nutrients, total alkalinity, dissolved inorganic carbon and dissolved organic carbon of the European continental rivers for the years 1977–2002. Inst. of Oceanography, University of Hamburg, Germany. Berichte aus

dem Zentrum für Meeres- und Klimaforschung 48, 159.
Pollard, R.T., Griffiths, M.J., Cunningham, S.A., Read, J.F., Pérez, F.F., Ríos, A.F., 1996. Vivaldi 1991 - a study of the formation, circulation and ventilation of Eastern North Atlantic Central Water. Prog. Oceanogr. 37 (2), 167–192.
Radach, G., Lenhart, H.J., 1995. Nutrient dynamics in the North Sea: fluxes and budgets in the water column derived from ERSEM. Neth. J. Sea Res. 33 (3), 301–335.
Radach, G., Pätsch, J., 1997. Climatological annual cycles of nutrients and chlorophyll in the North Sea. J. Sea Res. 38 (3), 231–248.
Sallée, J.B., Shuckburgh, E., Bruneau, N., Meijers, A.J.S., Bracegirdle, T.J., Wang, Z., 2013. Assessment of Southern Ocean mixed layer depths in CMIP5 models: historical bias and forcing response. J. Geophys. Res. Oceans 118, 1845–1862.
Sarafanov, A., 2009. On the effect of the North Atlantic Oscillation on temperature and salinity of the subpolar North Atlantic intermediate and deep waters. ICES J. Mar. Sci. 66, 1448–1454.
Savchuk, O.P., Gustafsson, B.G., Medina, M.R., Sokolov, A.V., Wulff, F.V., 2012. External nutrient loads to the Baltic Sea 1970–2006. Baltic Nest Institute, Stockholm, Sweden. Technical Report. 5. pp. 22.
Schrum, C., 2017. Regional Climate Modeling and Air-Sea Coupling. Oxford Research Encyclopedia of Climate Science.
Schrum, C., Lowe, J., Meier, H.E.M., Grabemann, I., Holt, J., Mathis, M., Pohlmann, T., Skogen, M.D., Sterl, A., Wakelin, S., 2016. Projected Change - North Sea. In: Quante, M., Colijn, F. (Eds.), North Sea Region Climate Change Assessment. Springer Berlin - Heidelberg, pp. 175–217.
Sein, D., Mikolajewicz, U., Gröger, M., Fast, I., Cabos, I., Pinto, J., Hagemann, S., Semmler, T., Izquierdo, A., Jacob, D., 2015. Regionally coupled atmosphere-ocean-sea ice-marine biogeochemistry model ROM. Part I: Description and validation. J. Adv. Model. Earth Syst. 7, 268–304.
Sherwin, T.J., Williams, M.O., Turrell, W.R., Hughes, S.L., Miller, P.I., 2006. A description and analysis of mesoscale variability in the Färoe-Shetland Channel. J. Geophys. Res. Oceans 111, C03003.
Simpson, J.H., McCandliss, R.R., 2013. "The Ekman Drain": a conduit to the deep ocean for shelf material. Ocean Dyn. 63 (9), 1063–1072.
Simpson, J.H., Sharples, J., 2012. Introduction to the physical and biological oceanography of shelf seas. Cambridge University Press, Cambridge, U.K., pp. 424.
Six, K.D., Maier-Reimer, E., 1996. Effects of plankton dynamics on seasonal carbon fluxes in an ocean general circulation model. Global Biogeochem. Cycles 10, 559–583.
Steinacher, M., Joos, F., Frölicher, T.L., Bopp, L., Cadule, P., Cocco, V., Doney, S.C., Gehlen, M., Lindsay, K., Moore, J.K., Schneider, B., Segschneider, J., 2010. Projected 21st century decrease in marine productivity: a multi-model analysis. Biogeosciences 7, 979–1005.
Suga, T., Motoki, K., Aoki, Y., Macdonald, A.M., 2004. The North Pacific climatology of winter mixed layer and mode waters. J. Phys. Oceanogr. 34, 3–22.
Sweby, P.K., 1984. High resolution schemes using flux limiters for hyperbolic conservation laws. Siam J. Numer. Anal. 21, 995–1011.
Thomas, H., Bozec, Y., de Baar, H., Elkalay, K., Frankignoulle, M., Kühn, W., Lenhart, H., Moll, A., Pätsch, J., Radach, G., Schiettecatte, L.S., Borges, A.V., 2010. Carbon and nutrient budgets of the North Sea. In: Liu, K.K., Atkinson, L., Qui nones, R., Talaue-McManus, L. (Eds.), Carbon and nutrient fluxes in continental margins: a global synthesis. Springer, Berlin, pp. 346–355.
Thomas, H., Bozec, Y., de Baar, H.J.W., Elkalay, K., Frankignoulle, M., Schiettecatte, L.-S., Kattner, G., Borges, A.V., 2005. The carbon budget of the North Sea. Biogeosciences 2, 87–96.
Thomas, M., Sündermann, J., Maier-Reimer, E., 2001. Consideration of ocean tides in an OGCM and impacts on subseasonal to decadal polar motion excitation. Geophys. Res. Lett. 28, 2457–2460.
Tian, T., Su, J., Boberg, F., Yang, S., Schmitt, T., 2016. Estimating uncertainty caused by ocean heat transport to the North Sea: experiments downscaling EC-EARTH. Clim. Dyn. 46 (1), 99–110.
Tinker, J., Lowe, J., Pardaens, A., Holt, J., Barciela, R., 2016. Uncertainty in climate projections for the 21st century northwest European shelf seas. Prog. Oceanogr. 148, 56–73.
Valcke, S., 2013. The OASIS3 coupler: a European climate modelling community software. Geosci. Model Dev. 6, 373–388.
Van Beusekom, J., Diel-Christiansen, A., 1994. Synthesis of Phyto- and Zooplankton Dynamics in the North Sea Environment. WWF International Report, World Wide Fund For Nature, Godalming. pp. 148 pp.
Varela, R.A., Cruzado, A., Gabaldon, J.E., 1995. Modelling primary production in the North Sea using the European Regional Seas Ecosystem Model. Neth. J. Sea Res. 33, 337–361.
Vermaat, J.E., McQuatters-Gollop, A., Eleveld, M.A., Gilbert, A.J., 2008. Past, present and future nutrient loads of the North Sea: causes and consequences. Estuar. Coast. Shelf Sci. 80 (1), 53–59.
Wakelin, S., Daewel, U., Schrum, C., Holt, J., Butenschön, M., Artioli, Y., Beecham, J., Lynam, C., Mackinson, S., 2012. MEECE deliverable D3.4: synthesis report for climate simulations, Part 3: NE Atlantic/North Sea. pp. 82. www.meece.eu/documents/deliverables/WP3/D3\%204_Part3_NE\%20Atlantic.pdf.
Wakelin, S.L., Artioli, Y., Butenschön, M., Allen, J.I., Holt, J.T., 2015. Modelling the combined impacts of climate change and direct anthropogenic drivers on the ecosystem of the northwest European continental shelf. J. Mar. Syst. 152, 51–63.
White, M., Bowyer, P., 1997. The shelf-edge current north-west of Ireland. Ann. Geophys. 15 (8), 1076–1083.
Wilcock, P., 2004. Sediment Transport Seminar. University of California at Berkeley, Lectures 1 and 3. . http://calm.geo.berkeley.edu/geomorph/wilcock/wilcock.html.
Williams, R.G., Follows, M.J., 2003. Physical transport of nutrients and the maintenance of biological production. In: Fasham, M. (Ed.), Ocean Biogeochemistry: The Role of the Ocean Carbon Cycle in Global Change, pp. 19–51 New York.
Williams, R.G., McDonagh, E., Roussenov, V.M., Torres-Valdes, S., King, B., Sanders, R., Hansell, D.A., 2011. Nutrient streams in the North Atlantic: advective pathways of inorganic and dissolved organic nutrients. Glob. Biogeochem. Cycles 25, 16.
Williams, R.G., McLaren, A., Follows, M.J., 2000. Estimating the convective supply of nitrate and implied variability in export production. Glob. Biogeochem. Cycles 14, 1299–1313.
Williams, R.G., Roussenov, V., Follows, M.J., 2006. Nutrient streams and their induction into the mixed layer. Glob. Biogeochem. Cycles 20, GB1016.
Woollings, T., Franzke, C., Hodson, D.L.R., Dong, B., Barnes, E.A., Raible, C.C., Pinto, J.G., 2015. Contrasting interannual and multidecadal NAO variability. Clim. Dyn. 45, 539–556.
Yool, A., Popova, E.E., Coward, A.C., 2015. Future change in ocean productivity: is the Arctic the new Atlantic? J. Geophys. Res. Oceans Atmos. 120 (12), 7771–7790.